Contribution of syndecans to the cellular entry of SARS-CoV-2

Anett Hudák
Pharmacoidea Ltd.
László Szilák
Pharmacoidea Ltd. https://orcid.org/0000-0003-0334-272X
Tamás Letoha (tamas.letoha@pharmacoidea.eu)
Pharmacoidea Ltd. https://orcid.org/0000-0002-6035-4009

Research Article

Keywords: coronaviruses, SARS-CoV-2, spike protein, cellular entry, syndecans

Posted Date: September 2nd, 2020

DOI: https://doi.org/10.21203/rs.3.rs-70340/v1

Version of Record: A version of this preprint was published at International Journal of Molecular Sciences on September 2nd, 2020. See the published version at https://doi.org/10.3390/ijms22105336.

Abstract

The severe acute respiratory syndrome coronavirus 2 (SARS-CoV-2) is a novel emerging pathogen causing an unprecedented pandemic in 21st century medicine. Due to the significant health and economic burden of the current SARS-CoV-2 outbreak, there is a huge unmet medical need for novel interventions effectively blocking SARS-CoV-2 infection. Unknown details of SARS-CoV-2 cellular biology significantly hamper the development of potent and highly specific SARS-CoV-2 therapeutics. Angiotensin-converting enzyme-2 (ACE2) has been reported to be the primary receptor for SARS-CoV-2 cellular entry. However, emerging scientific evidence suggests the involvement of additional membrane proteins, such as heparan sulfate proteoglycans, in SARS-CoV-2 internalization. Here we report that syndecans, the evolutionarily conserved family of transmembrane proteoglycans facilitate the cellular entry of SARS-CoV-2. Among syndecans, syndecan-4 was the most efficient in mediating SARS-CoV-2 uptake, yet overexpression of other isoforms, including the neuronal syndecan-3, also increased SARS-CoV-2 internalization. The S1 subunit of the SARS-CoV-2 spike protein plays a dominant role in the virus's interactions with syndecans. Besides the polyanionic heparan sulfate chains - the established binding sites for several viruses - other parts of the syndecan ectodomain, such as the cell-binding domain, also contribute to the interaction with SARS-CoV-2. During virus internalization, syndecans colocalize with ACE2, suggesting a jointly shared internalization pathway. Both ACE2 and syndecan inhibitors exhibited significant efficacy in reducing cellular entry of SARS-CoV-2, thus supporting the complex nature of internalization. Among these inhibitors, a peptide compromising the spike protein's heparin-binding PRRAR motif significantly reduced SARS-CoV-2 cellular uptake, highlighting the need to go beyond the ACE2 paradigm for developing efficient therapeutics against SARS-CoV-2. Data obtained on syndecan specific in vitro assays present syndecans as novel cellular targets of SARS-CoV-2 and offers molecularly precise, yet simple strategies in overcoming the complex nature of SARS-CoV-2 infection.

Introduction

The severe acute respiratory syndrome coronavirus 2 (SARS-CoV-2) is beta-coronavirus initially emerging in China and then rapidly spreading throughout the world, becoming a significant threat to human health[1-8]. On 13 March, the WHO declared Europe the epicenter of the SARS-CoV-2 pandemic[9]. Caused by SARS-CoV-2 infection, the coronavirus disease 2019 (COVID-19) poses specific challenges for adequate and effective treatment to avoid the onset of severe clinical manifestations[10]. Currently, there is no specific antiviral therapy against SARS-CoV-2 infection[11]. Several investigational agents have been described in observational studies or being used based on in vitro or extrapolated evidence[12,13]. Among the applied anti-COVID-19 therapeutics, remdesivir, an antiviral agent originally developed against Ebola infection, shows one of the most promising clinical efficacy in attenuating the severity of COVID-19[14,15]. Given the high mortality despite the use of remdesivir, novel, and more efficient combinatory strategies should be developed to improve patient outcomes in COVID-19[15].

Coronaviruses are endowed with a high tendency to spread from animals to humans, hence enabling cross- species transmission and facilitating severe outbreaks[5,16-19]. The capacity of coronaviruses for cross-species transmission also supports the need to develop highly efficient, yet safe therapeutics and prophylactics to tackle current and future pandemics[6,20-22].

Development of efficient therapeutics against COVID-19 is hampered by the unknown details of SARS-CoV- 2 cellular biology, which is greatly postulated on previous studies with SARS-CoV, a coronavirus strain responsible for the first SARS outbreak in 2002-2003[10]. Exploring the precise molecular events driving SARS-CoV-2 infection is critical for the development of novel and specific medicines against COVID-19.

SARS-CoV-2 is transmitted by multiple means, including liquid droplets, aerosol particles and fomites[23,24]. Once SARS-CoV-2 enters the nasal cavity, it binds to epithelial cells and migrates down the respiratory tract while triggering a robust immune response[10,25]. The angiotensin-converting enzyme 2 (ACE2) has been identified as the primary entry receptor for both SARS-CoV-2 and SARS-CoV[10,26-28]. However, scientific evidence shows that endocytosis of SARS-CoV also occurs through a novel, clathrin- and caveolae-independent endocytic pathway, mediated by attachment to cell surface heparan sulfate proteoglycans (HSPGs)[29-32]. Meanwhile, it has been also revealed that the S1 subunit of the SARS-CoV-2 spike protein, the subunit responsible for cellular attachment, contains the heparin-binding core motif PRRAR[33-36] (Supplementary Fig. S1). According to most recent models for SARS- CoV-2 infection, viral attachment and infection involve the formation of a complex between heparan sulfate (HS) and ACE2[37].

HSPGs are glycoproteins containing one or more covalently attached HS chains, a type of glycosaminoglycan (GAG)[38,39]. The evolutionarily highly conserved syndecans (SDCs) are the only transmembrane HSPG family and possess essential roles in cell interactions, adhesion, migration and signaling[40-42]. SDCs share a similar structure: a one-span and highly conserved transmembrane domain (TM) and a relatively short cytoplasmic domain (CD)[43,44]. The extracellular domain (ectodomain) of SDCs is more diverse, containing HS attachment sites with glycosaminoglycan (GAG) side chains[45,46]. Through their highly sulfated GAG chains, SDCs interact with a myriad of extracellular ligands, hence transmitting extracellular signals intracellularly[40,45-48]. Besides cell signaling, SDCs also mediate the intracellular transport of ligands[45-47]. During SDC-mediated endocytosis, ligand-mediated clustering of SDCs induces the redistribution of SDCs to lipid rafts and stimulation of a lipid raft-dependent, but clathrin- and caveolae- independent endocytosis of the SDC-ligand complex[46,47,49]. As ligands internalized through SDC-mediated endocytosis can avoid lysosomal degradation, several parasites, including viruses and bacteria, utilize SDCs as shuttles to enter the cells[50-56].

Members of the SDC family show tissue-specific expression: SDC1 is expressed on epithelial and plasma cells, SDC2 on endothelial cells, SDC3 in the neurons, while SDC4 is more ubiquitous[43,44,53,57]. The BioGPS gene expression database (http://biogps.org) indicates a high expression of SDC4 in human lung cells[53,58]. In the lung, SDCs contribute to the balanced progression of inflammation[59]. During SARS-CoV

and SARS-CoV-2 infection, certain chemokines such as CXCL10 might be predictive of the subsequent clinical course[60]. CXCL10 and SDC4 display a close interaction during lung inflammation, while SDC1 is essential to limit inflammation and lung injury after influenza infection[61-63]. Viruses targeting SDCs in the lung could thus interfere with SDC-dependent signaling, hence influencing the inflammatory response triggered by the infection. The involvement of SDC4 in the regulation of antiviral signaling has also been reported[56]. In their excellent paper, Lin et al. meticulously demonstrated the SDC4 inducing effect of a viral infection, along with SDC4's influence on attenuating antiviral immunity[56].

Our research group has been focusing on the exploration of SDCs' drug delivery and therapeutic potential. Our related studies with non-viral drug delivery agents, including cell-penetrating peptides (CPPs) and cationic liposomes, contributed to the understanding of SDCs' capacity to deliver bioactive macromolecules into the cells[43,44,64]. Moreover, we also revealed that SDCs contribute to the seeding and prion-like spreading of pathological protein aggregates, the major molecular culprits responsible for the onset of neurodegenerative disorders[45,46]. During these endeavors, we have been developing several SDC specific assays and constructs, enabling thorough analyses of SDCs' interactions with potential ligands. Considering the scientific evidence on the potential involvement of SDCs in SARS- CoV-2 infection, we progressed to explore the interaction of both SARS-CoV-2 and its spike protein S1 subunit (spikeS1) with SDC isoforms. Our SDC specific transfectants enabled the quantitative analysis of SDCs' contribution to the cellular entry of SARS-CoV-2, while structural SDC mutants allowed to examine the interaction of the virus and its spikeS1 with various parts of the SDC ectodomain. Besides SDC specific transfectants, our studies also included the lung-specific A549 cell line that, due to its relative resistance against ACE2-mediated SARS-CoV infection, poses a challenge to the current ACE2 paradigm[65].

Overall, our findings present SDCs as important contributors to SARS-CoV-2 cellular entry and highlight the interplay of SDCs with ACE2 during the cellular uptake of the virus. Exploration of the complex molecular interplay driving SARS-CoV-2 cellular entry also helped us to identify novel inhibitors of virus internalization.

Results

SDCs facilitate cellular uptake of the SARS-CoV-2. SDC isoforms were created in K562 cells, a human myeloid leukemia cell line lacking endogenous HSPGs except for minor amounts of endogenous betaglycan[55]. K562 cells also express no detectable levels of caveolin-1, the main component of caveolae[66]. Due to their limited HSPG expression and inability to form caveolae, the source of caveolar endocytosis, K562 cells offer ideal cellular models to study the contribution of SDCs to cellular uptake of ligands without the interfering effects of other HSPGs or caveolae-mediated endocytosis[45,46]. As HS has already been established as a major binding site for several viruses[52], including SARS- CoV[32], stable SDC transfectants created in K562 cells were standardized according to their HS content[45,46]. (It's worth noting that SDC transfection did not induce statistically significant changes in ACE2 expression [Supplementary Fig. S2]). Thus, SDC transfectants with an equal amount of HS expression were selected and, along with

WT K562 cells, treated with heat-inactivated SARS-CoV-2 (at 1 MOI). After 18 h of incubation, cellular uptake of the virus was detected by incubating the SARS-CoV-2-treated, fixed and permeabilized cells with Alexa Fluor 488 (AF 488) labeled antibodies specific for SARS-CoV-2's spike glycoprotein. For imaging flow cytometry analyses, surface-attached SARS-CoV-2 was removed with trypsinization (according to the method of Nakase et al.), hence enabling the measurement of the internalized viral particles only[67]. Imaging flow cytometry analyses revealed increased uptake of SARS-CoV-2 into SDC transfectants (Figs. 1a-c). Among SDCs, SDC4 increased SARS-CoV-2 uptake the most ($p<0.01$). (Incubating the cells with the AF 488-labeled secondary antibodies did not result in any statistically significant difference in cellular fluorescence of applied WT K562 cells and SDC transfectants, showing that no unspecific binding influenced the detected difference in fluorescence intensities of SARS-CoV-2-treated cells [Supplementary Fig. S3]). Colocalization studies revealed a significant degree of colocalization between SARS-CoV- 2 and SDCs, suggesting the same route SDCs and SARS-CoV-2 follow during cellular entry (Figs. 1d and e). Namely, the Mander's overlap coefficients (MOC) for SDCs and SARS-CoV-2 were around 0.8, an indicator of significant colocalization (Fig. 1e). Colocalization of SARS-CoV-2 with SDCs during virus entry was also confirmed with imaging flow cytometry (Fig. 1d). The Bright Detail Similarity (BDS) score of colocalization between the fluorescent signals of the SDCs and SARS-CoV-2 also showed a high degree of colocalization (generally, a BDS score of 2 or greater represents a high degree of overlap [68]), especially in SDC3 and 4 transfectants (Fig. 1d).

Contribution of various parts of the SDC4 ectodomain to SARS-CoV-2 uptake. Studies on isoform-specific SDC cell lines demonstrated that SDCs increase cellular uptake of SARS-CoV-2. Among SDCs, SDC4 facilitated cellular uptake of SARS-CoV-2 the most. To investigate the molecular mechanisms driving SARS-CoV-2's interaction with the SDC4 ectodomain, heat-inactivated SARS-CoV-2 (at 1 MOI) was incubated with transfectants expressing various SDC4 structural mutants (Fig. 2a). Deletion mutant Si4 possesses a truncated SDC4 extracellular domain made of only the short signal sequence (Si), while mutant CBD has a mutated ectodomain containing only the cell-binding domain (CBD) and Si, but no HS attachment (HSA) site and HS chains[43-46]. We also applied the deletion mutant HSA with an ectodomain comprising the HSA site and HS chains (and also the Si), but no CBD[43-46]. To readily detect their expression, all of the SDC4 mutants – along with WT SDC4 – were tagged with GFP and expressed in K562 cells[43-46]. (As shown in Supplementary S4, expression of the SDC4 mutants did not influence ACE2 expression.) Clones with an equal extent of SDC expression were selected and treated with SARS-CoV-2. After incubation, the cells were trypsinized to remove extracellularly attached viral particles[67]. The cells were then fixed, permeabilized and treated with fluorescently (AF 647) labeled antibodies specific for spike glycoprotein of SARS-CoV-2. Fluorescence was then analyzed with imaging flow cytometry and confocal microscopy. Imaging flow cytometry revealed that both the HSA and CBD of SDC4 has a significant role in interacting with SARS-CoV-2 (Figs. 2b-d). Namely, deleting both the CBD and the HSA with HS chains reduced cellular uptake of SARS-CoV-2, as shown by the markedly reduced intracellular fluorescence detected on Si4 mutants (Figs. 2b-d). However, the insignificant reduction in the cellular fluorescence of SARS-CoV-2-treated CBD mutants showed that the CBD plays an important role in the interaction with the virus. Microscopic colocalization also showed marked colocalization of SARS-CoV-2

with either of the HSA or CBD mutants, with MOC values around 0.8 (Fig. 2e), demonstrating that SARS-CoV-2 could attach to both the HS chains or the CBD of SDC4. Contrary to CBD and HSA mutants, the MOC values measured on Si4 mutants showed significant (i.e. $p < 0.001$) reduction vs WT SDC4, thus highlighting the importance of CBD and HSA in the interactions with SARS-CoV-2. Overall, our studies with SDC4 deletion mutants revealed that besides the polyanionic HS chains, SARS-CoV-2 also interacts with the CBD of SDC4, highlighting the importance of the HS-independent parts of the SDC4 core protein. (Incubating the cells with the AF 633-labeled secondary antibodies did not induce any difference in fluorescence among the applied SDC4 transfectants and SDC4 mutants, showing that no unspecific binding influenced the difference in the detected fluorescence intensities in SARS-CoV-2-treated cells [Supplementary Fig. S5])

Cellular internalization of SARS-CoV-2 into A549 cells. After assessing the interaction of SARS-CoV-2 with the SDC4 ectodomain, we conducted studies on A549 cells, a human airway epithelia with a reportedly low level of endogenous ACE2 expression[65]. As transfection of ACE2 did not render to A549 cells to support SARS-CoV replication, A549 cells offer an ideal cellular model to study novel pathways for coronavirus entry[69]. Exploration of the SDC expression profile showed modest, yet detectable levels of SDCs in A549 cells (Figs. 3a and b). In terms of ACE2 expression, A549 cells express significantly less ACE2 then WT K562 cells, yet internalize heat-inactivated SARS-CoV-2 more efficiently (Figs. 3e-i), suggesting that ACE2 independent cellular modalities are also involved in the cellular uptake of SARS-CoV-2. Considering A549 cells' richer expression of SDCs (Figs. 3c and d), along with previous findings of increased SARS-CoV-2 uptake due to SDC overexpression, we also explored the involvement of SDCs in SARS-CoV-2 uptake on A549 cells. Imaging flow cytometry and confocal microscopy analyses demonstrated the high colocalization of SDCs with SARS-CoV-2 (Figs. 4a and b). ACE2, the established receptor for SARS-CoV- 2 also showed high colocalization with the virus in uptake studies on A549 cells (Figs. 4a and b). The next steps showed that ACE2 and SDCs colocalize during SARS-CoV-2 uptake, suggesting that ACE2 and SDCs collaborate in mediating SARS-CoV-2 internalization (Figs. 4c and d). Co-IP studies also confirmed SARS-CoV-2 binding SDC4, but also ACE2 (Supplementary Fig. S6).

SDCs facilitate cellular uptake of the SARS-CoV-2 spike protein S1 subunit. To widen the understanding of SARS-CoV-2's complex cellular entry, we also explored the cellular interactions of the SARS-CoV-2 spike protein S1 subunit (spikeS1), responsible for mediating attachment to host cells. At first, we explored the potential cellular uptake of spikeS1 into SDC transfectants created in K562 cells. Just like in the case of heat-inactivated SARS-CoV-2, SDC transfectants with an equal amount of HS expression were selected and, along with WT K562 cells, treated with spikeS1. After 18 h of incubation, cellular uptake was detected by incubating the spikeS1-treated, fixed and permeabilized cells with fluorescently (FITC) labeled antibody specific for the N-terminal His-tag of the recombinant spikeS1. For imaging flow cytometry analyses, extracellular fluorescence of surface-attached spikeS1 was removed with trypsinization (according to the method described by Nakase et al.)[67]. Imaging flow cytometry analyses revealed increased uptake of spikeS1 into SDC lines (Figs. 5a-c). Among SDCs, SDC4 significantly increased the uptake of spikeS1 ($p<0.01$). (Incubating the cells with the fluorescently labeled anti-His tag antibodies

without spikeS1 pretreatment did not induce any difference in fluorescence among the applied K562 cells and SDC transfectants, showing that no unspecific binding influenced the detected fluorescence intensities in spikeS1-treated cells [Supplementary Fig. S7]). Colocalization studies revealed a significant degree of colocalization between spikeS1 and SDC4, suggesting the same route SDC4 and spikeS1 follow during cellular entry (Figs. 5d and e). Namely, both the BDS and the MOC for SDC4 and spikeS1 were around 3 and 0.8, respectively, hence indicating significant colocalization (Figs. 5d and e).

Contribution of various parts of the SDC4 ectodomain to spikeS1 uptake. As both SARS-CoV-2 and spikeS1 demonstrated similarly increased internalization into SDC transfectants, suggesting that spikeS1 would be a key modality to facilitate SARS-CoV-2's interactions with SDCs, we also explored the interaction of spikeS1 with SDC4 structural mutants (Fig. 2a). Transfectants of GFP-tagged Si4, CBD and HSA and SDC4 were incubated with spikeS1 for 18 h. After incubation, the cells were fixed, permeabilized and treated with AF 647-labeled secondary antibodies specific for the N-terminal His-tag of spikeS1. Fluorescence was then analyzed with imaging flow cytometry and confocal microscopy. To remove extracellularly spikeS1, the trypsinization method of Nakase et al. was applied[67]. Just like in the case of SARS-CoV-2, both the HSA and CBD proved to serve a significant role in interacting with spikeS1. Namely, deleting both the CBD and the HSA (with HS chains) significantly reduced cellular uptake of spikeS1, as shown by the markedly reduced intracellular fluorescence detected on Si4 mutants (Figs. 6a-d). However, the insignificant reduction in the cellular fluorescence of spikeS1-treated CBD or HSA mutants showed that deleting either the CBD or the HS chains could not reduce the internalization of spikeS1 significantly (Fig. 6c). Thus, the CBD or the HSA site of SDC4 could compensate for the removal of either the HS chains or the CBD, respectively. In the case of the SDC4 transfectants and the HSA and CBD mutants, the Bright Detail Similarity (BDS) score of colocalization between the fluorescent signals of the SDC4 constructs and spikeS1 also showed a high degree of colocalization (Figs. 6c and d). Compared to SDC4 transfectants, the BDS score of Si4 mutants lacking HS chains and CBD were significantly reduced ($p<0.05$). Microscopic colocalization also showed marked colocalization of the spikeS1 with either of the HSA or CBD mutants, with MOC values around 0.8, demonstrating that spikeS1 could attach to both the HS chains or the CBD of SDC4 (Fig. 6e). Co-IP studies also confirmed the ability of the CBD or the HS chains of SDC4 to bind spikeS1 (Supplementary Fig. S8). Our studies with the SDC4 deletion mutants thus revealed that besides interacting with the polyanionic HS chains, spikeS1 also interacts with the CBD of SDC4. (Incubating the cells with the fluorescently labeled anti-His tag antibodies without spikeS1 pretreatment did not induce any difference in fluorescence among the applied SDC4 transfectants and SDC4 mutants, showing that no unspecific binding influenced the detected fluorescence intensities in spikeS1-treated cells [Supplementary Fig. S9])

Interaction of spikeS1 with SDC4 in A549 cells. Previous studies showed modest, yet detectable levels of SDC4 expression in A549 cells (Figs. 3a-d). As SDC4 demonstrated highest uptake efficacy of spikeS1, we created an SDC4 transfectant exhibiting elevated SDC4 expression (Figs. 7a and b). It's worth noting that SDC4 overexpression did not affect the modest expression of ACE2 in A549 cells (Supplementary Fig. S10). Increased SDC4 expression, with unaffected ACE2 levels, resulted in increased cellular uptake

of spikeS1 (Figs. 7c-g). Namely, overexpression of SDC4 increased spikeS1 entry from a low level of WT A549 cells by almost twofold (Fig. 7c-e). Colocalization studies revealed that spikeS1 colocalizes with SDC4 during increased spikeS1 entry (as shown by the high BDS and MOC scores obtained with imaging flow cytometry and confocal microscopy, see details in Figs. 7f and g, while co- immunoprecipitation showed increased binding of spikeS1 to SDC4 due to SDC4 overexpression [Fig. 7h]). (Incubating the cells with the fluorescently labeled anti-His tag antibodies without spikeS1 pretreatment did not induce any difference in fluorescence among the applied A549 cell line and SDC4 transfectants, showing that no unspecific binding influenced the detected fluorescence intensities in spikeS1-treated cells [Supplementary Fig. S11]).

Inhibitor studies support the complexity of SARS-CoV-2 uptake. Utilizing SDC transfectants and A549 cells, we managed to reveal an interplay of ACE2 and SDCs in mediating the cellular uptake of SARS-CoV-2. Developing efficient SARS-CoV-2 therapeutics requires the consideration of the complexity of SARS-CoV-2's cellular interplay. This complexity was also demonstrated in our studies with representative inhibitors of various cellular pathways. The following inhibitors were applied: amiloride hydrochloride (amiloride) as the well-established inhibitor of macropinocytosis[70]; DX600 as a selective ACE2 blocker[71]; Gö 6983 as a selective PKC antagonist[72-74]; heparin as the inhibitor of electrostatic interactions of GAGs[75]; a heparin-binding peptide (WQPPRARI, abbreviated as HBP) derived from fibronectin[76-78]; and a small peptide (SPRRAR) derived from the heparin binding motif of SARS-CoV-2. Among them, amiloride and heparin is considered as more general inhibitors, DX600 and Gö 6983 are selective. As PKC activation is required for triggering SDC-mediated uptake, the application of Gö 6983 served the exploration of SDCs in SARS-CoV-2 internalization. The HBP (WQPPRARI) from fibronectin competes to the attachment of HS chains of SDCs, while SPRRAR, derived from spikeS1 contains a very efficient heparin-binding motif. As shown in. Figs. 8a-c, uptake studies demonstrated that while all of the applied inhibitors efficiently reduced SARS-CoV-2 uptake, SPRRAR, a peptide derived from the spikeS1 of SARS-CoV-2 emerged as the most potent one, demonstrating that molecularly detailed understanding the of SARS-CoV-2 internalization could indeed lead to the rational development of potent SARS-CoV-2 therapeutic leads. (Preincubating the cells with the inhibitors did not influence cell viability, demonstrating that the reduced SARS-CoV-2 uptake due to inhibitor treatment did not arose from disturbed cellular viability [Supplementary Fig. S12]).

Discussion

The current outbreak of SARS-CoV-2, a novel coronavirus with a yet undetermined origin, causes an unprecedented threat to modern societies[5,79,80]. Due to the WHO declared SARS-CoV-2 pandemic, intense research is being manifested to deliver specific medicines halting virus spread and infection[12]. Pharmaceutical efforts in delivering efficient, yet safe medicines against SARS-CoV-2 are being hampered by the unknown details of SARS-CoV-2 cellular biology[10,81]. While most studies on SARS-CoV-2 emphasize the difference between SARS-CoV-2 and SARS-CoV, several findings on SARS-CoV are also being regarded as applicable for SARS-CoV-2[82]. One such fundamental finding on SARS-CoV that has

been widely accepted for SARS-CoV-2 is ACE2 serving as the primary, yet sole cellular entry receptor, facilitating virus internalization after transmembrane protease serine type 2 (TMPRSS2) mediated cleavage of the spike protein[27,28,83,84]. However, the failure of highly specific ACE2 pharmaceuticals to stop SARS-CoV-2 infection and related disease, COVID-19, clearly highlights the complexity of SARS-CoV-2 internalization[85]. Emerging evidence show the collaboration of ACE2 and HSPGs during SARS-CoV-2 uptake[37].

It has been widely accepted that cell surface HSPGs provide efficient cellular entry for a whole range of pathogens[50-52]. SDCs are the only transmembrane family of HSPGs[38,39]. Due to their versatile and polyanionic HS chains, SDCs bind a myriad of extracellular ligands, including several viruses. Due to their evolutionary conserved intracellular PDZ domains, SDCs also interact with a whole range of intracellular signaling molecules, thus providing a transmembrane link between extracellular HS-mediated processes and intracellular signaling cascades[40,42,47,86]. Attachment to HS chains of HSPGs and interaction with PDZ domains has been already explored for SARS-CoV, but not yet investigated for SARS-CoV-2[29,30,32]. However, recent studies explored the interaction of the SARS-CoV-2 with heparin[87]. According to these studies, the conformation change induced by the attachment of spikeS1 to heparin is required for efficient SARS-CoV-2 entry into the cells[87]. Another very recent findings of also showed heparin effectively blocking SARS-CoV-2 invasion into Vero cells[88]. It has to be noted that the primary sequence of spikeS1 (namely Pro681 - Arg685) contains the heparin-binding core motif PRRAR[33-35] (Supplementary Fig. S1). According to current reports, this heparin-binding motif may facilitate SARS-CoV-2 host cell entry[36].

Considering scientific evidence supporting the involvement of HSPGs in SARS-CoV-2 infection, we set up a study exploring the contribution of SDCs to the cellular uptake of SARS-CoV-2 and spikeS1, the subunit responsible for cell attachment of the virus. Up-till-now, this is the first study exploring the specific involvement of the whole SDC family in the cellular uptake of SARS-CoV-2. According to our results, the overexpression of SDCs, including SDC4, the isoform most abundant in the lung, significantly increases cellular uptake of SARS-CoV-2. Thus, SDCs have a key involvement in facilitating the cellular entry of SARS-CoV-2, while the spikeS1 plays a major role in the interactions with SDCs. Binding of SARS-CoV-2 to the SDC4 ectodomain is not exclusively driven by the HS chains, but also influenced by other parts of the SDC ectodomain, including SDC4's CBD mediating cell-to-cell attachment. In our studies with SDC4 deletion mutants, the CBD mutants lacking HS chains exhibited internalization characteristics comparable to WT SDC4 transfectants, thus supporting the involvement of the SDC core protein in the interaction with the virus. SDC4's CBD also played a dominant role in spikeS1-SDC4 interactions, hence emphasizing the need to go beyond standard HS-virus interactions in understanding the molecular interplay between SARS-CoV-2 and SDCs. In our studies, heparin, a polyanionic agent effectively inhibiting the attachment of several viruses to polyanionic HS on cell surface proteoglycans[52], even at very high doses, did not emerged as the most potent blocker of virus uptake, while SPRRAR, a heparin-binding peptide derived from spikeS1 showed superior efficacy to block virus uptake.

It's worth noting that the sulfation pattern of proteoglycans, contributing significantly to the structural diversity of proteoglycan HS chains, defines the binding of ligands[38,45,48,89-91]. Although most cells express more than one HSPG at their cell surface, several lines of evidence indicate that HS chains attached to different core proteins on the same cell surface have the same sulfation patterns[39,92-94]. The detected difference in the cellular uptake of SARS- CoV-2 (and also spikeS1) between various SDC transfectants expressing similar level of HS also indicates that interaction of SARS-CoV-2 with SDCs is also influenced by HS independent parts of the SDC core protein. Investigating the cellular uptake of SARS-CoV-2 in stable SDC transfectants with an equal amount of HS expression was therefore critical in understanding the influence of the core protein (i.e. the non-GAG parts) on interactions with the virus. As the fine structure and ligand binding of SDCs' HS chains show cell type-specific differences[94-96], the involvement of different cell lines in the analyses of SDCs interaction with SARS-CoV-2s was also crucial in the exploration of factors influencing the virus' cellular interactions.

Exploration of SARS-CoV-2 internalization in A549 cells also revealed the interplay of SDCs and ACE2, where both modalities (i.e. ACE2 and SDCs) interact with SARS-CoV-2 to facilitate its cellular entry. Therefore, our results do not abolish the ACE2 hypothesis, but depicts a molecularly more diverse scenario involving the collaboration of SDCs and ACE2 in mediating SARS-CoV-2 internalization. The finding that SDC overexpression, with unaffected ACE2 expression levels, results in increased SARS-CoV-2 cellular entry highlights the importance of SDCs in the complex molecular interplay of SARS-CoV-2 internalization.

SDCs have been already regarded as a favorite binding site for several viruses and bacteria[51,52]. In line with these findings, our results suggest that SDCs play a key role in facilitating SARS-CoV-2's cellular entry. Although most abundant in the lungs, the widespread distribution of SDC4 and other SDCs in the human body can explain the ability of SARS-CoV-2 the spread to various organs. Also, the increased uptake of SARS-CoV-2 into cells expressing other SDCs, including neuronal SDC3 might imply the virus's ability to infect the cells of the CNS. Considering the ability of HIV-1 to exploit SDCs to enter the brain[97], our finding on the increased uptake of SARS-CoV-2 into SDC3 transfectants might explain the molecular determinants of SARS-CoV-2's potential CNS entry[98]. Moreover, altered expression of SDCs is associated with cardiovascular disorders, diabetes, obesity and Alzheimer's disease, just some of the most common comorbidities correlating with poorer clinical outcomes in COVID-19[99-107].

Overall, our results obtained in highly specific SDC assays presents SDCs as important mediators of SARS- CoV-2 cellular entry and highlight SDCs, including the lung abundant SDC4, as a novel therapeutic target against SARS-CoV-2 infection. Our findings are in line with recent reports suggesting the potential role of HSPGs in the cellular entry of SARS-CoV-2 and explore a molecularly more detailed interplay of ACE2 and SDCs in facilitating SARS-CoV-2 uptake. Inhibitor studies show the efficacy of inhibitors of both pathways (i.e. ACE2 or SDC-dependent) in blocking SARS-CoV-2 internalization, while highlighting the efficacy of peptide (SPRRAR) derived from the heparin-binding motif of SARS-CoV-2. Pharmaceutical development of efficient medicines against SARS-CoV-2 infection therefore should consider a more

complex interplay of potential receptors in order to develop efficient mono- or combinatorial therapeutic strategies against SARS-CoV-2 infection.

Materials And Methods

Heat-inactivated SARS-CoV-2, recombinant proteins and peptides. Heat-inactivated SARS-CoV-2 (strain: 2019- nCoV/USA-WA1/2020) was purchased from ATCC® (cat. no. ATCC® VR-1986HK™), the N-terminally His-tagged recombinant SARS-CoV-2 Spike Protein S1 Subunit (region Val16 - Gln690) from RayBiotech, recombinant human syndecan-4 from R&D Systems (cat. no. 2918-SD) and recombinant human ACE2 from Abcam (ab151852). Peptide inhibitors utilized for the studies were purchased from either BACHEM (DX600) or Genscript (SPRRAR and WQPPRARI).

SDC constructs, cell culture and transfection. Full-length SDC1-4 and SDC4 deletion mutants and transfectants, established in K562 cells (ATCC® CCL-243™), were created as described previously [43,45,46]. No His-tags were applied for the SDC constructs. SDC4 overexpressing A549 clones, along with WT A549 cells (ATCC® CCL-185™) were then grown in Advanced MEM medium (Thermo Fischer Scientific) supplemented with 10% FCS (Gibco) at 37 °C in a humified 5% CO2 containing air environment.

Flow cytometry analysis of HS, ACE2 and SDC expression. HS and SDC expression of applied cell lines (WT K562 and SDC transfectants) were measured with flow cytometry by using anti-human HS antibody (10E4 epitope [Amsbio]), AF 488-labeled anti-mouse IgM and APC-labeled antibody, as described previously[45,46]. SDC transfectants with almost equal amount of HS expression were selected for further uptake studies. ACE2 expression of WT K562 and A549 cells, along with SDC transfectants was measured with human ACE-2 AF 647-conjugated antibody (R&D Systems, cat. no. FAB9332R) according to the manufacturer's protocol.

Flow cytometry analysis of SARS-CoV-2 and spikeS1 uptake. WT K562 and A549 cells, SDC transfectants, along with SDC4 structural mutants were utilized to quantify internalization of spikeS1. Briefly, 6 x 10^5 cells/ml in DMEM/F12 medium were incubated with either SARS-CoV-2 (at 1 MOI) or spikeS1 (at a concentration of 2 µg/ml) for 18 h at 37 ºC. After 18 h of incubation, the cells were trypsinized (with the method described by Nakase et al [67]) to remove the extracellularly attached virus particles or spikeS1 from the cell surface. Then the cells were washed, fixed, permeabilized and blocked with the appropriate serum for 1h at room temperature. In case of spikeS1, the cells were then treated with fluorescently (either FITC or in case of SDC4 mutants, AF 647) labeled anti-His-tag antibodies (rabbit poly- and monoclonal, Abcam, cat. no. ab1206 and ab237337) for 1 h. In case of SARS-CoV-2, the cells were then treated with mouse monoclonal (1A9) to SARS spike glycoprotein (Abcam, cat.no: 273433), followed by treatment with either AF 488- (SDC transfectants and A549 cells) or AF 633-labeled (SDC mutants) goat anti-mouse IgG (both Invitrogen, cat.no.: A-11001 and A-21052, respectively). For the colocalization studies, SDCs made visible by incubating the cells with either APC-labeled SDC or AF-labeled antibodies (1:100), while ACE2 was detected by using either AF 647-labeled human ACE2 antibody (R&D systems, cat.no: FAB9332R) or rabbit polyclonal Ace2 antibody (Abcam, cat.no.

ab272690) and fluorescently (FITC) labeled anti-rabbit antibody (Sigma). The samples were then rinsed three times with PBS containing 1% BSA and 0.1% Triton X-100, and progressed towards flow cytometry. Cellular uptake was then measured by flow cytometry using an AMNIS® FlowSight imaging flow cytometer (AMNIS Corporation). A minimum of 10,000 events per sample was analyzed. Appropriate gating in a forward-scatter-against- side-scatter plot was utilized to exclude cellular debris and aggregates. Fluorescence analysis was conducted with the IDEAS™ analysis software. To examine the influence of the fluorescently labeled anti-His-tag antibodies or secondary IgGs, some of the cells were also treated with either anti-His-tag or secondary antibodies without preincubation with spikeS1 or SARS-CoV-2 and cellular fluorescence was measured with imaging flow cytometry.

Inhibitor studies. To reveal the involvement of various endocytosis pathways, A549 cells were preincubated with the following inhibitors 30 min before SARS-CoV-2 admission: amiloride hydrochloride (at a concentration of 100 μM) as the well-established inhibitor of micropinocytosis (Sigma); DX600 as a selective ACE2 blocker (10 μM; BACHEM); Gö 6983 as a selective PKC antagonist (10 μM; Sigma); heparin as the inhibitor of electrostatic interactions of GAGs (200 ug/ml; Sigma); a heparin-binding peptide (WQPPRARI, 100 μM; Genscript) derived from fibronectin; SPRRAR derived from spikeS1 (100 μM; Genscript). After incubation with these inhibitors, the cells were treated with SARS-CoV-2 and processed for the flow cytometric analyses as described above.

Cell viability measurements. The effect of the applied inhibitors were assessed by incubating A549 cells were with either of the following inhibitors: amiloride hydrochloride (amiloride, at a concentration of 100 μM), DX600 (10 μM); Gö 6983 (10 μM, Sigma); heparin (200 ug/ml); a heparin-binding peptide (WQPPRARI) and SPRRAR (100 μM). Eighteen hours after incubation with these inhibitors, viability of inhibitor-treated WT A549 cells, along with untreated controls, were assessed with the EZ4U Cell Proliferation Assay (Biomedica Gmbh, cat. no. BI-5000) according to the instructions of the manufacturer. Absorbance was measured with a BioTek Cytation 3 multimode microplate-reader.

Microscopic visualization of uptake. The internalization of SARS-CoV-2 or spikeS1 was visualized by confocal microscopy. WT A549 and WT K562 cells, along with SDC transfectants and SDC4 mutants were grown on poly-D- lysine-coated glass-bottom 35-mm culture dishes (MatTek Corp.). After 24 h, the cells were preincubated in DMEM/F12 medium at 37 °C for 30 min before incubation with the spikeS1 at a concentration of 2 μg/ml. After incubation with either SARS-CoV-2 (1MOI) or spikeS1, the cells were rinsed two times with ice-cold PBS, fixed in 4% paraformaldehyde (Sigma), the cell membranes were permeabilized (0,1% Triton X-100), and the cells were blocked with the appropriate serum for 1h at room temperature, followed by the specific antibody treatments as described for the flow cytometry analyses. The samples were then rinsed three times with PBS containing 0.1% Triton X-100, then stained with DAPI (1:5000) for 5 min, washed three times with PBS and embedded in Fluoromount G (SouthernBiotech)[45,46]. The distribution of fluorescence was then analyzed on a Leica DMi8 microscope equipped with Aurox Clarity Laser Free Confocal Unit. Sections presented were taken approximately at the mid-height level of the cells. Photomultiplier gain and illumination power were identical within each experiment. The Aurox Visionarysoftware was used for image acquisition by confocal microscopy. For colocalization analyses,

the images were analyzed in the ImageJ software (NIH, Bethesda, Maryland, US) with the plug-in JACoP as described by Wesén et al.[108] 12 images (18 images per sample, experiments performed in triplicate) were analyzed, and the data is presented as mean ± SEM.

Co-immunoprecipitation experiments. SDC4 transfectants or WT K562 or A549 cells, incubated with or without SARS-CoV2 or spikeS1 (as mentioned above), were processed for co-immunoprecipitation experiments as described previously[45,46]. Briefly, after incubation, the cells were washed twice with ice-cold PBS and treated with cold Pierce IP lysis buffer. Then the cells were scraped off to clean Eppendorf tubes, put on a low-speed rotating shaker for 15 min and centrifuged at 14,000 g for 15 min at 4°C. The supernatant was then transferred to new tubes and combined with 5 µg of either of mouse monoclonal (1A9) SARS-Cov2 spike glycoprotein S1 antibody (Abcam, cat. no. ab273433) or, in the case of the GFP-tagged SDC4 mutants, GFP antibody (Abcam, cat. no. ab6662). The antigen sample/SDC/SARS-CoV-2 or GFP antibody mixture was then incubated for overnight at 4°C with mixing. The antigen sample/antibody mixture was then added to a 1.5 ml microcentrifuge tube containing pre-washed Pierce Protein A/G Magnetic Beads (Thermo Fisher Scientific) and after incubation at room temperature for 1 hour with mixing, the beads were then collected with a MagJET Separation Rack magnetic stand (Thermo Fisher Scientific) and supernatants were discarded. To eluate the antigen, 100µl of SDS-PAGE reducing sample buffer were then added to the tubes and samples were heated at 96°C for 10 minutes in 1% SDS and the samples were proceeded to SDS-PAGE[45,46]. The samples were then immunoblotted onto PVDF membranes and the proteins were detected with specific antibodies as described above. Image acquisition was conducted with Uvitec's Alliance Q9 Advanced Imaging Platform.

Statistical analysis. Results are expressed as means ± standard error of the mean (SEM). Differences between experimental groups were evaluated by using one-way analysis of variance (ANOVA). Values of $p<0.05$ were accepted as significant[45,46]. During imaging flow cytometry, the IDEAS™ feature Bright Detail Similarity (BDS) was used to measure colocalization between two signals[68]. A BDS score of 2 or greater represents a high degree of overlap. For microscopic colocalization analyses, the Mander's overlap coefficient (MOC) was calculated as described by Wesen et al.[108]

Declarations

Acknowledgements

AH, LS and TL have received funding from the Innovative Medicines Initiative 2 Joint Undertaking under grant agreement No 807015. This Joint Undertaking receives support from the European Union's Horizon 2020 research and innovation programme and EFPIA. AH, LS and TL have been also supported by grants EUREKA_16-1-2017- 0018 and 2017-2.3.6-TÉT-CN-2018-00023 of the National Research, Development and Innovation Office, Hungary. AH, LS and TL have also received funding from grant GINOP-2.1.2-8-1-4-16-2017-00234.

Author contributions statement

TL conceived the project, while TL and AH performed the experimental work and analyzed data and drafted the manuscript. LS constructed the SDC plasmids. All authors have approved the final article.

Additional information

Competing interests: The authors declare no competing interests.

References

1. El Zowalaty, M. E. & Jarhult, J. D. From SARS to COVID-19: A previously unknown SARS- related coronavirus (SARS-CoV-2) of pandemic potential infecting humans - Call for a One Health approach. *One Health* **9**, 100124, doi:10.1016/j.onehlt.2020.100124 (2020).
2. Chu, D. K. W. *et al.* Molecular Diagnosis of a Novel Coronavirus (2019-nCoV) Causing an Outbreak of Pneumonia. *Clin Chem* **66**, 549-555, doi:10.1093/clinchem/hvaa029 (2020).
3. Coronaviridae Study Group of the International Committee on Taxonomy of, V. The species Severe acute respiratory syndrome-related coronavirus: classifying 2019-nCoV and naming it SARS-CoV-2. *Nat Microbiol* **5**, 536-544, doi:10.1038/s41564-020-0695-z (2020).
4. Malik, S. *et al.* Emerging novel coronavirus (2019-nCoV)-current scenario, evolutionary perspective based on genome analysis and recent developments. *Vet Q* **40**, 68-76, doi:10.1080/01652176.2020.1727993 (2020).
5. Boni, F. *et al.* Evolutionary origins of the SARS-CoV-2 sarbecovirus lineage responsible for the COVID-19 pandemic. *Nat Microbiol*, doi:10.1038/s41564-020-0771-4 (2020).
6. Shereen, M. A., Khan, S., Kazmi, A., Bashir, N. & Siddique, R. COVID-19 infection: Origin, transmission, and characteristics of human coronaviruses. *J Adv Res* **24**, 91-98, doi:10.1016/j.jare.2020.03.005 (2020).
7. Zheng, SARS-CoV-2: an Emerging Coronavirus that Causes a Global Threat. *Int J Biol Sci* **16**, 1678-1685, doi:10.7150/ijbs.45053 (2020).
8. Zhu, N. *et al.* A Novel Coronavirus from Patients with Pneumonia in China, 2019. *N Engl J Med* **382**, 727- 733, doi:10.1056/NEJMoa2001017 (2020).
9. Chan, J. F. *et al.* A familial cluster of pneumonia associated with the 2019 novel coronavirus indicating person-to-person transmission: a study of a family cluster. *Lancet* **395**, 514-523, doi:10.1016/S0140- 6736(20)30154-9 (2020).
10. Mason, R. J. Pathogenesis of COVID-19 from a cell biology perspective. *Eur Respir J* **55**, doi:10.1183/13993003.00607-2020 (2020).
11. Li, , Liu, S. M., Yu, X. H., Tang, S. L. & Tang, C. K. Coronavirus disease 2019 (COVID-19): current status and future perspectives. *Int J Antimicrob Agents*, 105951, doi:10.1016/j.ijantimicag.2020.105951

(2020).

12. Tu, Y. F. *et al.* A Review of SARS-CoV-2 and the Ongoing Clinical Trials. *Int J Mol Sci* **21**, doi:10.3390/ijms21072657 (2020).
13. Gabutti, G., d'Anchera, E., Sandri, F., Savio, M. & Stefanati, A. Coronavirus: Update Related to the Current Outbreak of COVID-19. *Infect Dis Ther*, 1-13, doi:10.1007/s40121-020-00295-5 (2020).
14. Warren, T. K. *et al.* Therapeutic efficacy of the small molecule GS-5734 against Ebola virus in rhesus monkeys. *Nature* **531**, 381-385, doi:10.1038/nature17180 (2016).
15. Beigel, J. H. *et al.* Remdesivir for the Treatment of Covid-19 - Preliminary Report. *N Engl J Med*, doi:10.1056/NEJMoa2007764 (2020).
16. Lau, S. K. & Chan, J. F. Coronaviruses: emerging and re-emerging pathogens in humans and animals. *Virol J* **12**, 209, doi:10.1186/s12985-015-0432-z (2015).
17. Ye, Z. W. *et al.* Zoonotic origins of human coronaviruses. *Int J Biol Sci* **16**, 1686-1697, doi:10.7150/ijbs.45472 (2020).
18. Bolles, M., Donaldson, E. & Baric, R. SARS-CoV and emergent coronaviruses: viral determinants of interspecies transmission. *Curr Opin Virol* **1**, 624-634, doi:10.1016/j.coviro.2011.10.012 (2011).
19. Xu, J. *et al.* Systematic Comparison of Two Animal-to-Human Transmitted Human Coronaviruses: SARS- CoV-2 and SARS-CoV. *Viruses* **12**, doi:10.3390/v12020244 (2020).
20. Guo, Y. R. *et al.* The origin, transmission and clinical therapies on coronavirus disease 2019 (COVID-19) outbreak - an update on the status. *Mil Med Res* **7**, 11, doi:10.1186/s40779-020-00240-0 (2020).
21. Yan, Y. *et al.* The First 75 Days of Novel Coronavirus (SARS-CoV-2) Outbreak: Recent Advances, Prevention, and Treatment. *Int J Environ Res Public Health* **17**, doi:10.3390/ijerph17072323 (2020).
22. Kock, R. A. *et al.* 2019-nCoV in context: lessons learned? *Lancet Planet Health* **4**, e87-e88, doi:10.1016/S2542-5196(20)30035-8 (2020).
23. Meselson, M. Droplets and Aerosols in the Transmission of SARS-CoV-2. *N Engl J Med* **382**, 2063, doi:10.1056/NEJMc2009324 (2020).
24. Jayaweera, M., Perera, H., Gunawardana, B. & Manatunge, J. Transmission of COVID-19 virus by droplets and aerosols: A critical review on the unresolved dichotomy. *Environ Res* **188**, 109819, doi:10.1016/j.envres.2020.109819 (2020).
25. Zou, *et al.* SARS-CoV-2 Viral Load in Upper Respiratory Specimens of Infected Patients. *N Engl J Med* **382**, 1177-1179, doi:10.1056/NEJMc2001737 (2020).
26. Wan, Y., Shang, J., Graham, R., Baric, R. S. & Li, F. Receptor Recognition by the Novel Coronavirus from Wuhan: an Analysis Based on Decade-Long Structural Studies of SARS Coronavirus. *J Virol* **94**, doi:10.1128/JVI.00127-20 (2020).
27. Hoffmann, M. *et al.* SARS-CoV-2 Cell Entry Depends on ACE2 and TMPRSS2 and Is Blocked by a Clinically Proven Protease Inhibitor. *Cell* **181**, 271-280 e278, doi:10.1016/j.cell.2020.02.052 (2020).
28. Hofmann, H. & Pohlmann, S. Cellular entry of the SARS coronavirus. *Trends Microbiol* **12**, 466-472, doi:10.1016/j.tim.2004.08.008 (2004).

29. Lang, J. *et al.* Inhibition of SARS pseudovirus cell entry by lactoferrin binding to heparan sulfate proteoglycans. *PLoS One* **6**, e23710, doi:10.1371/journal.pone.0023710 (2011).
30. Vicenzi, E. *et al.* Coronaviridae and SARS-associated coronavirus strain HSR1. *Emerg Infect Dis* **10**, 413- 418, doi:10.3201/eid1003.030683 (2004).
31. Owczarek, K. *et al.* Early events during human coronavirus OC43 entry to the cell. *Sci Rep* **8**, 7124, doi:10.1038/s41598-018-25640-0 (2018).
32. Wang, H. *et al.* SARS coronavirus entry into host cells through a novel clathrin- and caveolae-independent endocytic pathway. *Cell Res* **18**, 290-301, doi:10.1038/cr.2008.15 (2008).
33. Anand, , Puranik, A., Aravamudan, M., Venkatakrishnan, A. & Soundararajan, V. SARS-CoV-2 selectively mimics a cleavable peptide of human ENaC in a strategic hijack of host proteolytic machinery. *bioRxiv*, 2020.2004.2029.069476, doi:10.1101/2020.04.29.069476 (2020).
34. Wijelath, S. *et al.* Heparin-II domain of fibronectin is a vascular endothelial growth factor-binding domain: enhancement of VEGF biological activity by a singular growth factor/matrix protein synergism. *Circ Res* **99**, 853-860, doi:10.1161/01.RES.0000246849.17887.66 (2006).
35. Coutard, B. *et al.* The spike glycoprotein of the new coronavirus 2019-nCoV contains a furin-like cleavage site absent in CoV of the same *Antiviral Res* **176**, 104742, doi:10.1016/j.antiviral.2020.104742 (2020).
36. Kim, S. Y. *et al.* Glycosaminoglycan binding motif at S1/S2 proteolytic cleavage site on spike glycoprotein may facilitate novel coronavirus (SARS-CoV-2) host cell entry. *bioRxiv*, 2020.2004.2014.041459, doi:10.1101/2020.04.14.041459 (2020).
37. Clausen, T. M. *et al.* SARS-CoV-2 Infection Depends on Cellular Heparan Sulfate and ACE2. *bioRxiv*, doi:10.1101/2020.07.14.201616 (2020).
38. Sarrazin, S., Lamanna, W. C. & Esko, J. D. Heparan sulfate proteoglycans. *Cold Spring Harb Perspect Biol* **3**, doi:10.1101/cshperspect.a004952 (2011).
39. Lindahl, U., Couchman, J., Kimata, K. & Esko, J. D. in *Essentials of Glycobiology* (eds rd *et al.*) 207-221 (2015).
40. Tkachenko, E., Rhodes, J. M. & Simons, M. Syndecans: new kids on the signaling block. *Circ Res* **96**, 488- 500, doi:10.1161/01.RES.0000159708.71142.c8 (2005).
41. Couchman, J. R. Transmembrane signaling proteoglycans. *Annu Rev Cell Dev Biol* **26**, 89-114, doi:10.1146/annurev-cellbio-100109-104126 (2010).
42. Choi, Y., Chung, H., Jung, H., Couchman, J. R. & Oh, E. S. Syndecans as cell surface receptors: Unique structure equates with functional diversity. *Matrix Biol* **30**, 93-99, doi:10.1016/j.matbio.2010.10.006 (2011).
43. Letoha, T. *et al.* Cell-penetrating peptide exploited syndecans. *Biochim Biophys Acta* **1798**, 2258-2265, doi:10.1016/j.bbamem.2010.01.022 (2010).
44. Letoha, *et al.* Contribution of syndecans to lipoplex-mediated gene delivery. *Eur J Pharm Sci* **49**, 550-555, doi:10.1016/j.ejps.2013.05.022 (2013).

45. Hudak, A. *et al.* Contribution of syndecans to cellular uptake and fibrillation of alpha-synuclein and tau. *Sci Rep* **9**, 16543, doi:10.1038/s41598-019-53038-z (2019).
46. Letoha, T. *et al.* Contribution of syndecans to cellular internalization and fibrillation of amyloid-beta(1-42). *Sci Rep* **9**, 1393, doi:10.1038/s41598-018-37476-9 (2019).
47. Christianson, C. & Belting, M. Heparan sulfate proteoglycan as a cell-surface endocytosis receptor. *Matrix Biol* **35**, 51-55, doi:10.1016/j.matbio.2013.10.004 (2014).
48. Kramer, L. & Yost, H. J. Heparan sulfate core proteins in cell-cell signaling. *Annu Rev Genet* **37**, 461-484, doi:10.1146/annurev.genet.37.061103.090226 (2003).
49. Payne, K., Jones, S. A., Chen, C. & Zhuang, X. Internalization and trafficking of cell surface proteoglycans and proteoglycan-binding ligands. *Traffic* **8**, 389-401, doi:10.1111/j.1600-0854.2007.00540.x (2007).
50. Bartlett, A. H. & Park, P. W. Proteoglycans in host-pathogen interactions: molecular mechanisms and therapeutic implications. *Expert Rev Mol Med* **12**, e5, doi:10.1017/S1462399409001367 (2010).
51. Cagno, , Tseligka, E. D., Jones, S. T. & Tapparel, C. Heparan Sulfate Proteoglycans and Viral Attachment: True Receptors or Adaptation Bias? *Viruses* **11**, doi:10.3390/v11070596 (2019).
52. Aquino, S. & Park, P. W. Glycosaminoglycans and infection. *Front Biosci (Landmark Ed)* **21**, 1260-1277, doi:10.2741/4455 (2016).
53. Zimmermann, N. *et al.* Syndecans promote mycobacterial internalization by lung epithelial cells. *Cell Microbiol* **18**, 1846-1856, doi:10.1111/cmi.12627 (2016).
54. Bacsa, S. *et al.* Syndecan-1 and syndecan-2 play key roles in herpes simplex virus type-1 infection. *J Gen Virol* **92**, 733-743, doi:10.1099/vir.0.027052-0 (2011).
55. Shafti-Keramat, S. *et al.* Different heparan sulfate proteoglycans serve as cellular receptors for human papillomaviruses. *J Virol* **77**, 13125-13135, doi:10.1128/jvi.77.24.13125-13135.2003 (2003).
56. Lin, W. *et al.* Syndecan-4 negatively regulates antiviral signalling by mediating RIG-I deubiquitination via CYLD. *Nat Commun* **7**, 11848, doi:10.1038/ncomms11848 (2016).
57. Woods, A., Oh, E. S. & Couchman, J. R. Syndecan proteoglycans and cell adhesion. *Matrix Biol* **17**, 477- 483, doi:10.1016/s0945-053x(98)90095-6 (1998).
58. Wu, C. *et al.* BioGPS: an extensible and customizable portal for querying and organizing gene annotation resources. *Genome Biol* **10**, R130, doi:10.1186/gb-2009-10-11-r130 (2009).
59. Gopal, S. Syndecans in Inflammation at a Glance. *Front Immunol* **11**, 227, doi:10.3389/fimmu.2020.00227 (2020).
60. Huang, C. *et al.* Clinical features of patients infected with 2019 novel coronavirus in Wuhan, China. *Lancet* **395**, 497-506, doi:10.1016/S0140-6736(20)30183-5 (2020).
61. Jiang, *et al.* Inhibition of pulmonary fibrosis in mice by CXCL10 requires glycosaminoglycan binding and syndecan-4. *J Clin Invest* **120**, 2049-2057, doi:10.1172/JCI38644 (2010).
62. Sato, *et al.* Baseline serum syndecan-4 predicts prognosis after the onset of acute exacerbation of idiopathic interstitial pneumonia. *PLoS One* **12**, e0176789, doi:10.1371/journal.pone.0176789

(2017).

63. Brauer, R. *et al.* Syndecan-1 Attenuates Lung Injury during Influenza Infection by Potentiating c-Met Signaling to Suppress Epithelial Apoptosis. *Am J Respir Crit Care Med* **194**, 333-344, doi:10.1164/rccm.201509-1878OC (2016).
64. Szilak, L., Letoha, T. & Ughy, B. What is the potential of syndecan-4-targeted novel delivery technologies? *Ther Deliv* **4**, 1479-1481, doi:10.4155/tde.13.112 (2013).
65. Jia, P. *et al.* ACE2 receptor expression and severe acute respiratory syndrome coronavirus infection depend on differentiation of human airway epithelia. *J Virol* **79**, 14614-14621, doi:10.1128/JVI.79.23.14614- 14621.2005 (2005).
66. Parolini, *et al.* Expression of caveolin-1 is required for the transport of caveolin-2 to the plasma membrane. Retention of caveolin-2 at the level of the golgi complex. *J Biol Chem* **274**, 25718-25725, doi:10.1074/jbc.274.36.25718 (1999).
67. Nakase, I. *et al.* Interaction of arginine-rich peptides with membrane-associated proteoglycans is crucial for induction of actin organization and macropinocytosis. *Biochemistry* **46**, 492-501, doi:10.1021/bi0612824 (2007).
68. Haridas, , Ranjbar, S., Vorobjev, I. A., Goldfeld, A. E. & Barteneva, N. S. Imaging flow cytometry analysis of intracellular pathogens. *Methods* **112**, 91-104, doi:10.1016/j.ymeth.2016.09.007 (2017).
69. Mossel, E. C. *et al.* Exogenous ACE2 expression allows refractory cell lines to support severe acute respiratory syndrome coronavirus replication. *J Virol* **79**, 3846-3850, doi:10.1128/JVI.79.6.3846-3850.2005 (2005).
70. Lin, X. P., Mintern, J. D. & Gleeson, P. A. Macropinocytosis in Different Cell Types: Similarities and Differences. *Membranes (Basel)* **10**, doi:10.3390/membranes10080177 (2020).
71. Pedersen, B., Sriramula, S., Chhabra, K. H., Xia, H. & Lazartigues, E. Species-specific inhibitor sensitivity of angiotensin-converting enzyme 2 (ACE2) and its implication for ACE2 activity assays. *Am J Physiol Regul Integr Comp Physiol* **301**, R1293-1299, doi:10.1152/ajpregu.00339.2011 (2011).
72. Young, L. H., Balin, B. J. & Weis, M. T. Go 6983: a fast acting protein kinase C inhibitor that attenuates myocardial ischemia/reperfusion injury. *Cardiovasc Drug Rev* **23**, 255-272, doi:10.1111/j.1527-3466.2005.tb00170.x (2005).
73. Gschwendt, M. *et al.* Inhibition of protein kinase C mu by various inhibitors. Differentiation from protein kinase c isoenzymes. *FEBS Lett* **392**, 77-80, doi:10.1016/0014-5793(96)00785-5 (1996).
74. Zeidman, R. *et al.* Novel and classical protein kinase C isoforms have different functions in proliferation, survival and differentiation of neuroblastoma cells. *Int J Cancer* **81**, 494-501, doi:10.1002/(sici)1097- 0215(19990505)81:3<494::aid-ijc26>3.0.co;2-l (1999).
75. Weiss, R. J., Esko, J. D. & Tor, Y. Targeting heparin and heparan sulfate protein interactions. *Org Biomol Chem* **15**, 5656-5668, doi:10.1039/c7ob01058c (2017).
76. Mooradian, D. L., McCarthy, J. B., Skubitz, A. P., Cameron, J. D. & Furcht, L. T. Characterization of FN-C/H-V, a novel synthetic peptide from fibronectin that promotes rabbit corneal epithelial cell adhesion, spreading, and motility. *Invest Ophthalmol Vis Sci* **34**, 153-164 (1993).

77. Wilke, M. S., Vespa, J., Skubitz, A. P., Furcht, L. T. & McCarthy, J. B. Human keratinocytes adhere to and spread on synthetic peptide FN-C/H-V derived from fibronectin. *J Invest Dermatol* **101**, 43-48, doi:10.1111/1523-1747.ep12358823 (1993).
78. Woods, A., McCarthy, J. B., Furcht, L. T. & Couchman, J. R. A synthetic peptide from the COOH-terminal heparin-binding domain of fibronectin promotes focal adhesion formation. *Mol Biol Cell* **4**, 605-613, doi:10.1091/mbc.4.6.605 (1993).
79. Lippi, & Plebani, M. The novel coronavirus (2019-nCoV) outbreak: think the unthinkable and be prepared to face the challenge. *Diagnosis (Berl)* **7**, 79-81, doi:10.1515/dx-2020-0015 (2020).
80. Fauci, A. S., Lane, H. C. & Redfield, R. R. Covid-19 - Navigating the Uncharted. *N Engl J Med* **382**, 1268- 1269, doi:10.1056/NEJMe2002387 (2020).
81. Yuen, K. S., Ye, Z. W., Fung, S. Y., Chan, C. P. & Jin, D. Y. SARS-CoV-2 and COVID-19: The most important research questions. *Cell Biosci* **10**, 40, doi:10.1186/s13578-020-00404-4 (2020).
82. Rabi, F. A., Al Zoubi, M. S., Kasasbeh, G. A., Salameh, D. M. & Al-Nasser, A. D. SARS-CoV-2 and Coronavirus Disease 2019: What We Know So Far. *Pathogens* **9**, doi:10.3390/pathogens9030231 (2020).
83. Shang, J. *et al.* Structural basis of receptor recognition by SARS-CoV-2. *Nature* **581**, 221-224, doi:10.1038/s41586-020-2179-y (2020).
84. Iwata-Yoshikawa, N. *et al.* TMPRSS2 Contributes to Virus Spread and Immunopathology in the Airways of Murine Models after Coronavirus Infection. *J Virol* **93**, doi:10.1128/JVI.01815-18 (2019).
85. Sungnak, W. *et al.* SARS-CoV-2 entry factors are highly expressed in nasal epithelial cells together with innate immune genes. *Nat Med*, doi:10.1038/s41591-020-0868-6 (2020).
86. Grootjans, J. J. *et al.* Syntenin, a PDZ protein that binds syndecan cytoplasmic domains. *Proc Natl Acad Sci U S A* **94**, 13683-13688, doi:10.1073/pnas.94.25.13683 (1997).
87. Mycroft-West, C. J. *et al.* Glycosaminoglycans induce conformational change in the SARS-CoV-2 Spike S1 Receptor Binding Domain. *bioRxiv*, 2020.2004.2029.068767, doi:10.1101/2020.04.29.068767 (2020).
88. Mycroft-West, C. J. *et al.* Heparin inhibits cellular invasion by SARS-CoV-2: structural dependence of the interaction of the surface protein (spike) S1 receptor binding domain with heparin. *bioRxiv*, 2020.2004.2028.066761, doi:10.1101/2020.04.28.066761 (2020).
89. El Masri, , Seffouh, A., Lortat-Jacob, H. & Vives, R. R. The "in and out" of glucosamine 6-O-sulfation: the 6th sense of heparan sulfate. *Glycoconj J* **34**, 285-298, doi:10.1007/s10719-016-9736-5 (2017).
90. Safaiyan, F., Lindahl, U. & Salmivirta, M. Selective reduction of 6-O-sulfation in heparan sulfate from transformed mammary epithelial cells. *Eur J Biochem* **252**, 576-582, doi:10.1046/j.1432-1327.1998.2520576.x (1998).
91. Turnbull, J., Powell, A. & Guimond, S. Heparan sulfate: decoding a dynamic multifunctional cell *Trends Cell Biol* **11**, 75-82, doi:10.1016/s0962-8924(00)01897-3 (2001).

92. Deepa, S., Yamada, S., Zako, M., Goldberger, O. & Sugahara, K. Chondroitin sulfate chains on syndecan- 1 and syndecan-4 from normal murine mammary gland epithelial cells are structurally and functionally distinct and cooperate with heparan sulfate chains to bind growth factors. A novel function to control binding of midkine, pleiotrophin, and basic fibroblast growth factor. *J Biol Chem* **279**, 37368-37376, doi:10.1074/jbc.M403031200 (2004).
93. Zako, *et al.* Syndecan-1 and -4 synthesized simultaneously by mouse mammary gland epithelial cells bear heparan sulfate chains that are apparently structurally indistinguishable. *J Biol Chem* **278**, 13561-13569, doi:10.1074/jbc.M209658200 (2003).
94. Kato, , Wang, H., Bernfield, M., Gallagher, J. T. & Turnbull, J. E. Cell surface syndecan-1 on distinct cell types differs in fine structure and ligand binding of its heparan sulfate chains. *J Biol Chem* **269**, 18881-18890 (1994).
95. Sanderson, D., Turnbull, J. E., Gallagher, J. T. & Lander, A. D. Fine structure of heparan sulfate regulates syndecan-1 function and cell behavior. *J Biol Chem* **269**, 13100-13106 (1994).
96. Hoffman, M. P. *et al.* Cell type-specific differences in glycosaminoglycans modulate the biological activity of a heparin-binding peptide (RKRLQVQLSIRT) from the G domain of the laminin alpha1 chain. *J Biol Chem* **276**, 22077-22085, doi:10.1074/jbc.M100774200 (2001).
97. Bobardt, D. *et al.* Contribution of proteoglycans to human immunodeficiency virus type 1 brain invasion. *J Virol* **78**, 6567-6584, doi:10.1128/JVI.78.12.6567-6584.2004 (2004).
98. Huang, J. *et al.* Potential of SARS-CoV-2 to Cause CNS Infection: Biologic Fundamental and Clinical Experience. *Front Neurol* **11**, 659, doi:10.3389/fneur.2020.00659 (2020).
99. Richardson, S. *et al.* Presenting Characteristics, Comorbidities, and Outcomes Among 5700 Patients Hospitalized With COVID-19 in the New York City Area. *JAMA*, doi:10.1001/jama.2020.6775 (2020).
100. Guan, W. J. *et al.* Comorbidity and its impact on 1590 patients with COVID-19 in China: a nationwide analysis. *Eur Respir J* **55**, doi:10.1183/13993003.00547-2020 (2020).
101. Kunnas, T. & Nikkari, S. T. Contribution of syndecan-4 genetic variants to hypertension, the TAMRISK study. *BMC Res Notes* **7**, 815, doi:10.1186/1756-0500-7-815 (2014).
102. Pessentheiner, A. R., Ducasa, G. M. & Gordts, P. Proteoglycans in Obesity-Associated Metabolic Dysfunction and Meta-Inflammation. *Front Immunol* **11**, 769, doi:10.3389/fimmu.2020.00769 (2020).
103. Han, J. & Hiebert, L. M. Alteration of endothelial proteoglycan and heparanase gene expression by high glucose, insulin and heparin. *Vascul Pharmacol* **59**, 112-118, doi:10.1016/j.vph.2013.08.001 (2013).
104. Schuring, A. N. *et al.* Role of syndecan-3 polymorphisms in obesity and female hyperandrogenism. *J Mol Med (Berl)* **87**, 1241-1250, doi:10.1007/s00109-009-0529-1 (2009).
105. Huang, W. H., Hwang, L. C., Chan, H. L., Lin, H. Y. & Lin, Y. H. Study of seven single-nucleotide polymorphisms identified in East Asians for association with obesity in a Taiwanese population. *BMJ Open* **6**, e011713, doi:10.1136/bmjopen-2016-011713 (2016).

106. Parveen, F. & Agrawal, S. A study of forty-seven single nucleotide polymorphisms among recurrent miscarriage using classification and regression tree analysis. *Am J Reprod Immunol* **70**, 529-537, doi:10.1111/aji.12152 (2013).
107. Liu, C. C. *et al.* Neuronal heparan sulfates promote amyloid pathology by modulating brain amyloid-beta clearance and aggregation in Alzheimer's disease. *Sci Transl Med* **8**, 332ra344, doi:10.1126/scitranslmed.aad3650 (2016).
108. Wesen, , Jeffries, G. D. M., Matson Dzebo, M. & Esbjorner, E. K. Endocytic uptake of monomeric amyloid- beta peptides is clathrin- and dynamin-independent and results in selective accumulation of Abeta(1-42) compared to Abeta(1-40). *Scientific reports* **7**, 2021, doi:10.1038/s41598-017-02227-9 (2017).

Figures

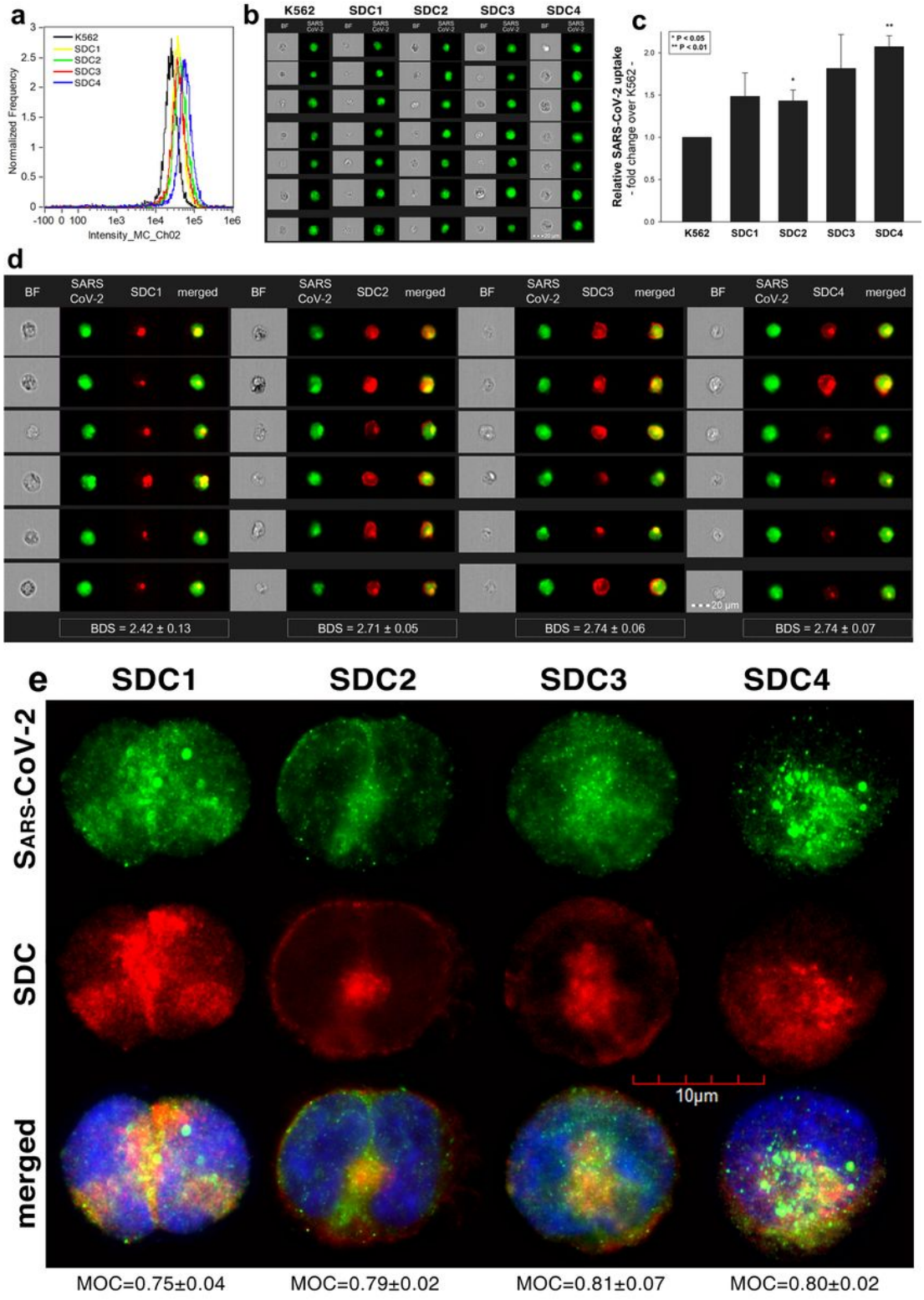

Figure 1

Cellular uptake of SARS-CoV-2 into SDC transfectants. WT K562 cells and SDC transfectants were incubated with heat-inactivated SARS-CoV-2 (at 1 MOI) for 18h at 37°C. After incubation, the cells were washed, trypsinized, fixed, permeabilized and treated with antibodies specific for the spike glycoprotein of SARS-CoV-2 (secondary antibody is labeled with AF 488) and, in the case of colocalization studies, APC-labeled SDC antibodies. Cellular uptake of SARS-CoV-2 was then analyzed with imaging flow cytometry

and confocal microscopy. (a-d) Results of imaging flow cytometry analyses. (a) Representative flow cytometry histograms showing the intracellular fluorescence of SARS-CoV-2-treated WT K562 cells and SDC transfectants. (b) Brightfield (BF) and fluorescent cellular images of SARS-CoV-2- treated WT K562 cells and SDC transfectants. Scale bar = 20 μm. (c) Detected fluorescence intensities were normalized to SARS-CoV-2-treated WT K562 cells as standards. The bars represent mean ± SEM of four independent experiments. Statistical significance vs standards (i.e. SARS-CoV-2-treated WT K562 cells) was assessed with analysis of variance (ANOVA). *$p<0.05$ vs standards; **$p<0.01$ vs standards. (d) Imaging flow cytometric analyses of SARS-CoV-2 (AF 488) and SDC (APC) colocalization. The indicated Bright Details Similarity (BDS) values of SARS-CoV-2 and SDCs represent mean ± SEM of four independent experiments. Statistical significance between the SDC transfectants was assessed with ANOVA (no statistically significant differences were detected). (e) Microscopic analyses of SARS-CoV-2 and SDC colocalization. Representative images of three independent experiments are shown. Scale bar = 10 μm. The Mander's overlap coefficient (MOC) ± SEM for the overlap of SDC with SARS-CoV-2 (indicated below the images) was calculated by analyzing 15 images with an average of 10 cells in each image (from 3 separate samples).

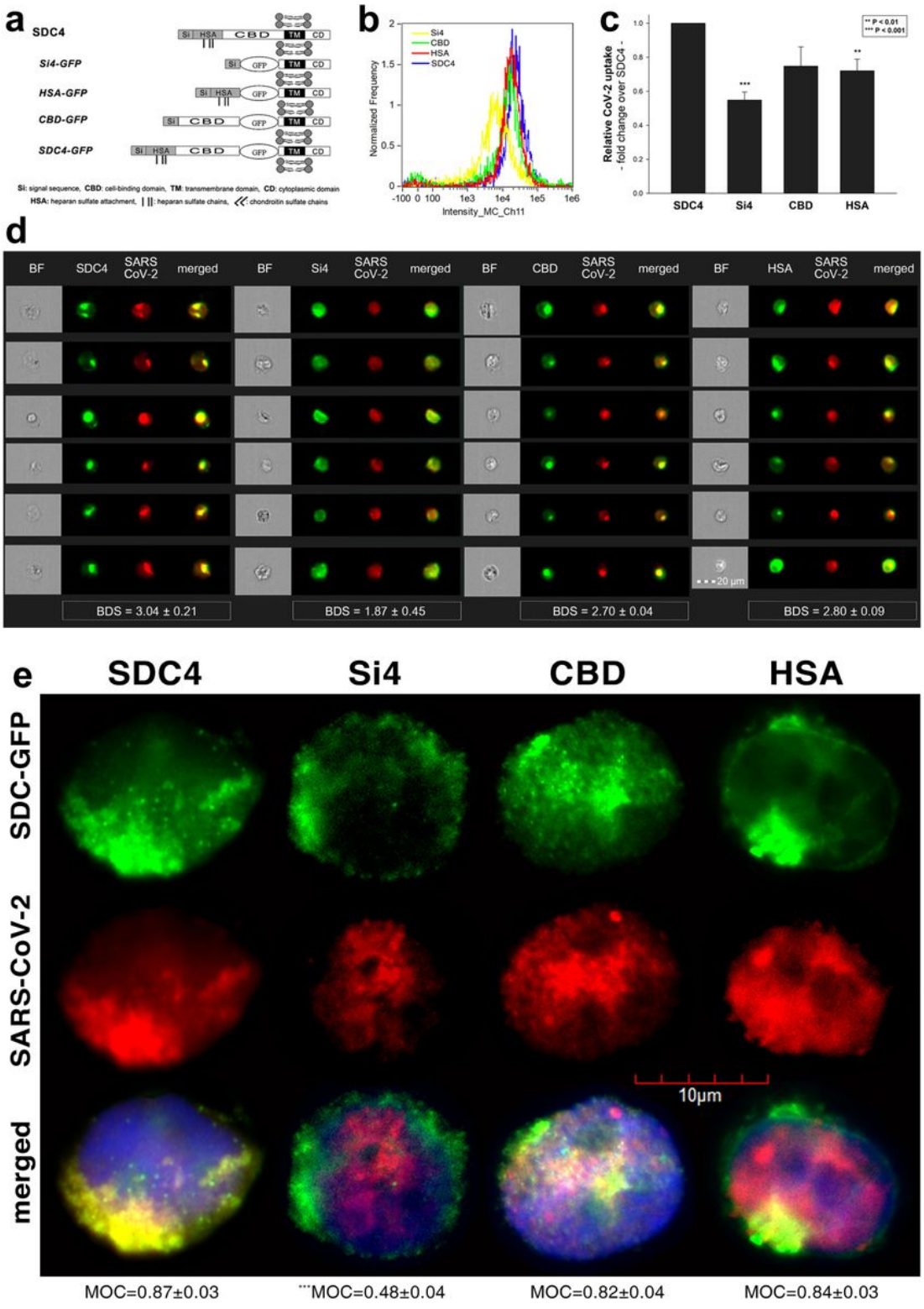

Figure 2

Contribution of the various parts of the SDC4 ectodomain to SARS-CoV-2 uptake. GFP-tagged SDC4 mutants incubated with SARS-CoV-2 (at 1 MOI) for 18 h were fixed, permeabilized and treated with specific and AF 633-labeled antibodies against SARS-CoV-2. Cellular uptake was then analyzed with imaging flow cytometry and confocal microscopy. (a) Schematic representation of the applied SDC4 mutants. (b-d) Results acquired with imaging flow cytometry. (b) Representative flow cytometry

histograms showing the intracellular fluorescence of SARS-CoV-2-treated SDC4 transfectants and mutants. (c) Detected fluorescence intensities were normalized to SARS-CoV-2-treated transfectants expressing WT SDC4 as standards. The bars represent mean ± SEM of four independent experiments. Statistical significance vs SARS-CoV-2-treated transfectants expressing WT SDC4 (standards) was assessed with ANOVA. **p<0.01 vs standards; ***p<0.01 vs standards. (d) BF and fluorescent images of SARS-CoV-2-treated SDC4 mutants. Scale bar = 20 μm. The indicated BDS values of SARS-CoV-2 and SDCs represent mean ± SEM of four independent experiments. Statistical significance between the SDC4 mutants was assessed with ANOVA. (e) Confocal microscopic visualization of SARS-CoV-2-treated SDC4, Si4, CBD and HSA transfectants. Scale bar = 10 μm. MOC ± SEM for the overlap of SARS-CoV-2 with SDC4, Si4, CBD and HSA (indicated below the images) was calculated by analysis of 15 images with ~10 cells in each image (from three separate samples). Statistical significance vs SARS-CoV-2-treated transfectants expressing WT SDC4 (standards) was assessed with ANOVA. ***p<0.001 vs standards (i.e. SARS-CoV-2-treated SDC4 transfectants).

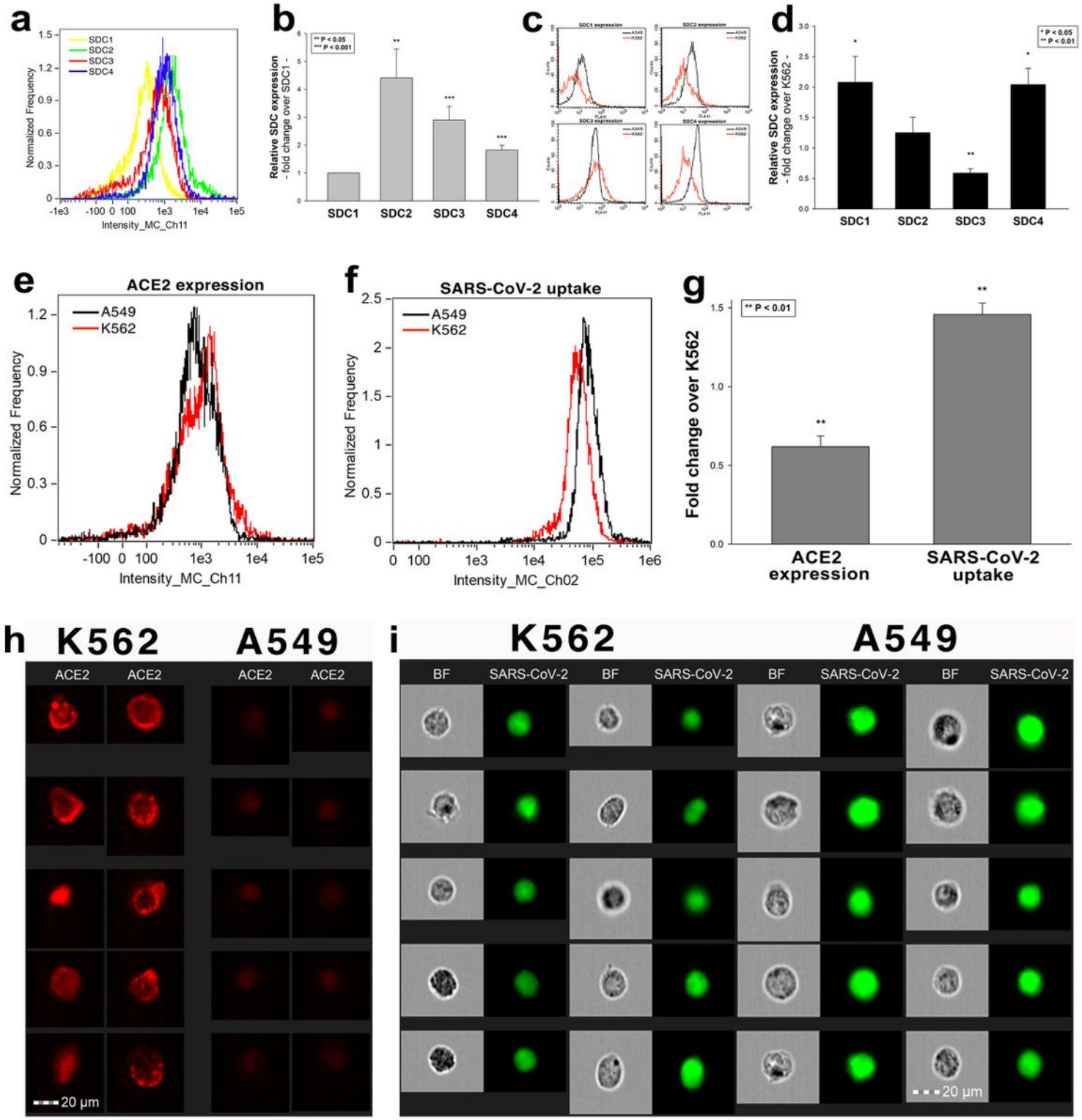

Figure 3

The difference of SARS-CoV-2 internalization in A549 and K562 cells. WT A549 and K562 cells were incubated with heat-inactivated SARS-CoV-2 (at 1 MOI) for 18h at 37°C. After incubation, the cells were washed, trypsinized, fixed, permeabilized and treated with antibodies specific for the spike glycoprotein of SARS-CoV-2 (secondary antibody is labeled with AF 488). Cellular uptake of SARS-CoV-2 was then analyzed with imaging flow cytometry. To investigate the effect of ACE2 and SDC expression on SARS-

CoV-2 uptake, ACE2 and SDC expression of WT A549 and K562 cells (all untreated with SARS-CoV-2) was also analyzed with flow cytometry by using fluorescently labeled antibodies specific for ACE2 and SDC isoforms. (a) Representative flow cytometry histograms showing the expression levels of SDC isoforms in WT A549 cells. (b) Detected SDC expression levels in A549 cells were normalized to that of SDC1. The bars represent mean ± SEM of nine independent experiments. Statistical significance vs SDC1 expression was assessed with ANOVA. **p<0.01 vs SDC1 expression; ***p<0.001 vs SDC1 expression. (c) Flow cytometry histograms representing the expression levels of SDC isoforms in WT A549 cells vs K562 cells. (d) Detected SDC expression levels in A549 cells were normalized to that of K562 cells as standards. The bars represent mean ± SEM of three independent experiments. Statistical significance vs K562 cells as standards was assessed with ANOVA. *p<0.05 vs K562 cells as standards; **p<0.01 vs K562 cells as standards. (e) Representative flow cytometry histograms showing the expression levels of ACE2 in WT K562 and A549 cells. (f) Representative flow cytometry histograms showing the intracellular fluorescence of SARS-CoV-2-treated WT K562 and A549 cells. (g) Detected ACE2 expression and SARS-CoV-2 internalization levels were normalized to those of WT K562 cells as standards. The bars represent mean ± SEM of three independent experiments. Statistical significance vs standards (WT K562 cells) was assessed with ANOVA. **p<0.01 vs standards. (h) Fluorescent images representing the ACE2 expression of K562 and A549 cells. Scale bar = 20 μm. (i) BF and fluorescent images of SARS-CoV-2-treated K562 and A549 cells. Scale bar = 20 μm.

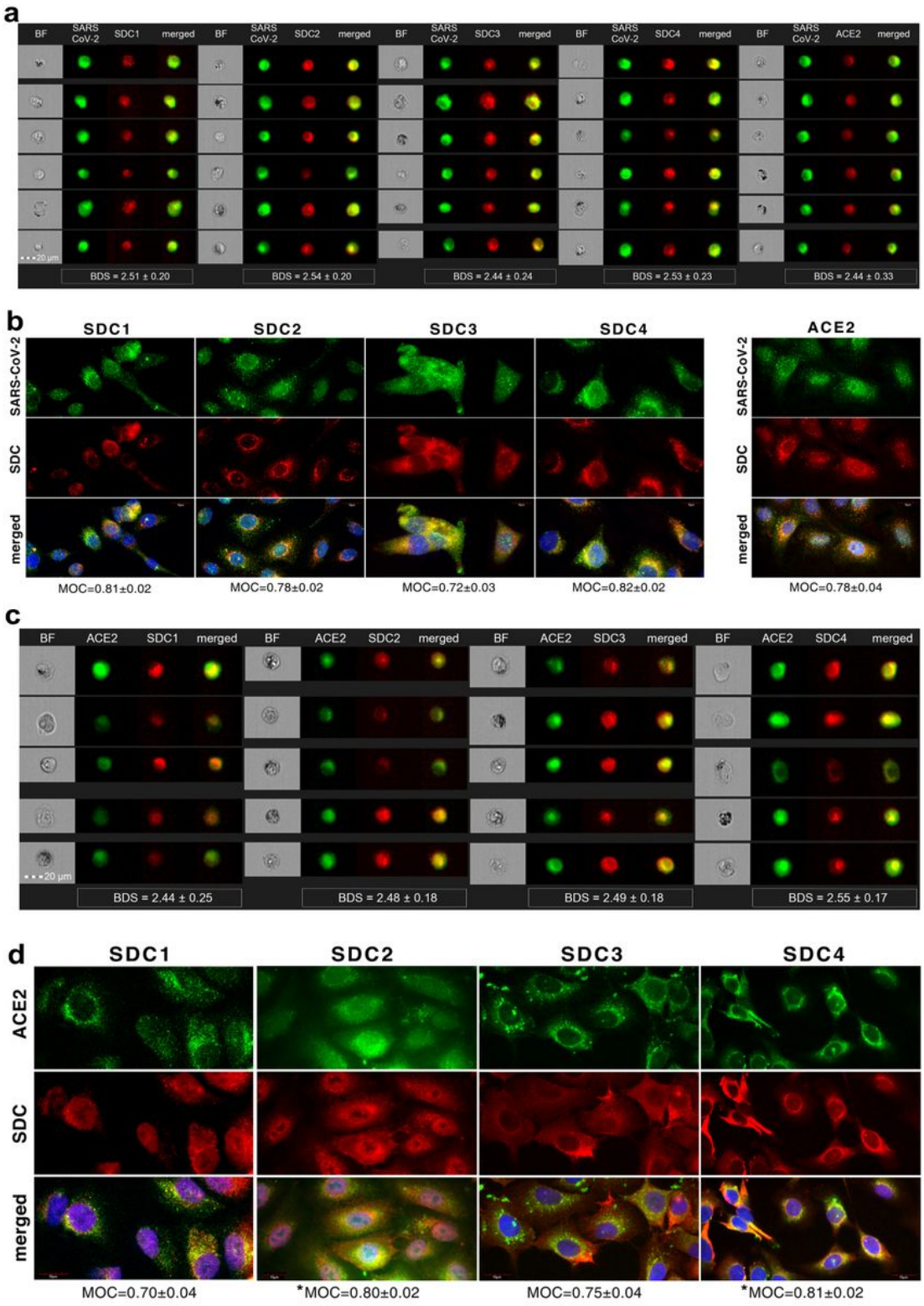

Figure 4

SARS-CoV-2 colocalizes with both SDCs and ACE2 during its uptake in A549 cells. WT A549 cells were incubated with heat-inactivated SARS-CoV-2 (at 1 MOI) for 18h at 37°C. After incubation, the cells were washed, trypsinized, fixed, permeabilized and treated with, in case of the SARS-CoV-2 / SDC colocalization studies, antibodies specific for the spike glycoprotein of SARS-CoV-2 (along with AF 488-labeled secondary antibody) and APC-labeled SDC antibodies. Colocalization of SARS-CoV-2 and ACE2

was analyzed by using AF 647-labeled antibody against ACE2. For analyzing colocalization between SDCs and ACE2, the SARS-CoV-2 treated cells, after incubation, were treated with AF 488-labeled antibodies against ACE2 and APC-labeled SDC antibodies. Colocalization of SARS-CoV-2 with SDCs and ACE2, or SDCs with ACE2 was then analyzed with imaging flow cytometry and confocal microscopy. (a) Imaging flow cytometry visualization of colocalization between SARS-CoV-2 and SDCs and ACE2 in SARS-CoV-2-treated A549 cells. Representative images of four independent experiments are shown. Scale bar = 20 μm. BDS of SARS-CoV-2 and SDCs (or ACE2) represent mean ± SEM of four independent experiments. Statistical significance between the groups was assessed with ANOVA (no statistically significant differences were detected). (b) Confocal microscopy visualization of colocalization between SARS-CoV-2 and SDCs or ACE2 in SARS-CoV-2-treated WT A549 cells. Representative images of four independent experiments are shown. Scale bar = 10 μm. MOC ± SEM for the overlap of SARS-CoV-2 with either of the SDC isoforms and ACE2 (indicated below each images) was calculated by analysis of 15 images with ~10 cells in each image (from three separate samples). (c) Imaging flow cytometry visualization of colocalization between ACE2 and SDCs in SARS-CoV-2-treated WT A549 cells. Representative images of four independent experiments are shown. Scale bar = 20 μm. The indicated BDS of ACE2 and SDCs represent mean ± SEM of four independent experiments. Statistical significance between the groups was assessed with ANOVA. No statistically significant differences were detected. (d) Confocal microscopy visualization of colocalization between ACE2 and SDCs in SARS-CoV-2-treated WT A549 cells. Representative images of four independent experiments are shown. Scale bar = 10 μm. MOC ± SEM for the overlap of ACE2 and SDCs (indicated below each images) was calculated by analysis of 15 images with ~10 cells in each image (from three separate samples). Statistical significance between the groups was assessed with ANOVA. MOC of ACE2 with SDC4 and SDC2 shows significant (*$p<0.05$) difference vs SDC1.

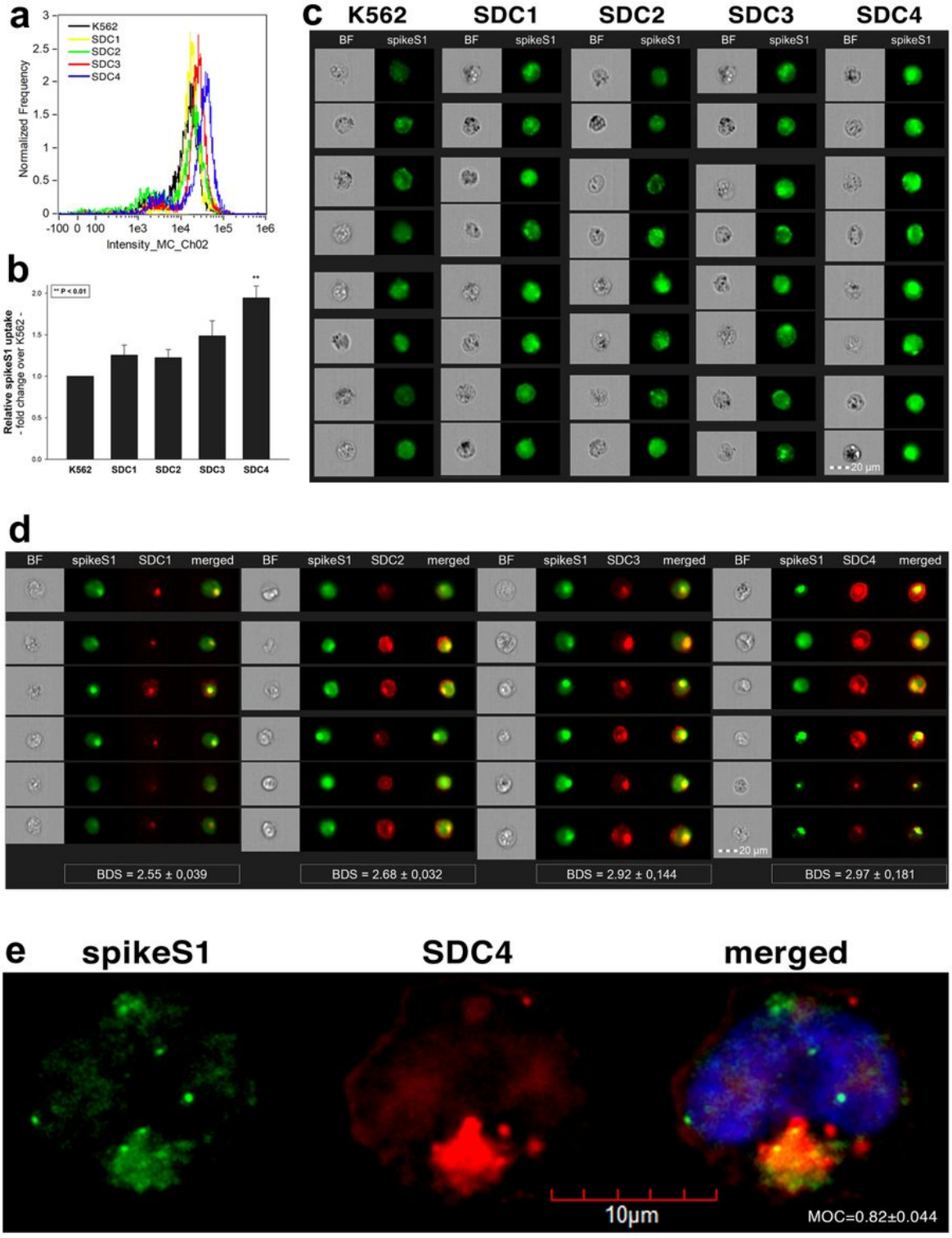

Figure 5

Cellular uptake of spikeS1 into SDC transfectants. WT K562 cells and SDC transfectants were incubated with spikeS1 for 18h at 37°C. After incubation, the cells were washed, trypsinized, fixed, permeabilized and treated with FITC-labeled antibodies specific for the N-terminal His-tag of the recombinant spikeS1. Cellular uptake of spikeS1 was then analyzed with imaging flow cytometry and confocal microscopy. (a-c) Results of imaging flow cytometry analyses. (a) A representative flow cytometry histogram showing

the intracellular fluorescence of spikeS1-treated WT K562 cells and SDC transfectants. (b) Detected fluorescence intensities were normalized to spikeS1-treated WT K562 cells as standards. The bars represent mean ± SEM of three independent experiments. Statistical significance vs standards was assessed with ANOVA. **p<0.01 vs standards. (c) BF and fluorescent cellular images of spikeS1-treated WT K562 cells and SDC transfectants. Scale bar = 20 μm (d) Imaging flow cytometry visualization of colocalization between SDCs and spikeS1. Representative images of four independent experiments are shown. Scale bar = 20 μm. The indicated BDS of spikeS1 and SDCs represent mean ± SEM of four independent experiments. Statistical significance between the groups was assessed with ANOVA. No statistically significant differences were detected. (e) Colocalization of spikeS1 and SDC4 detected with confocal microscopy. Representative images of three independent experiments are shown. Scale bar = 10 μm. MOC ± SEM for the overlap of SDC4 with spikeS1 (indicated on the image) was calculated by analyzing 12 images with an average of 12 cells in each image (from 3 separate samples).

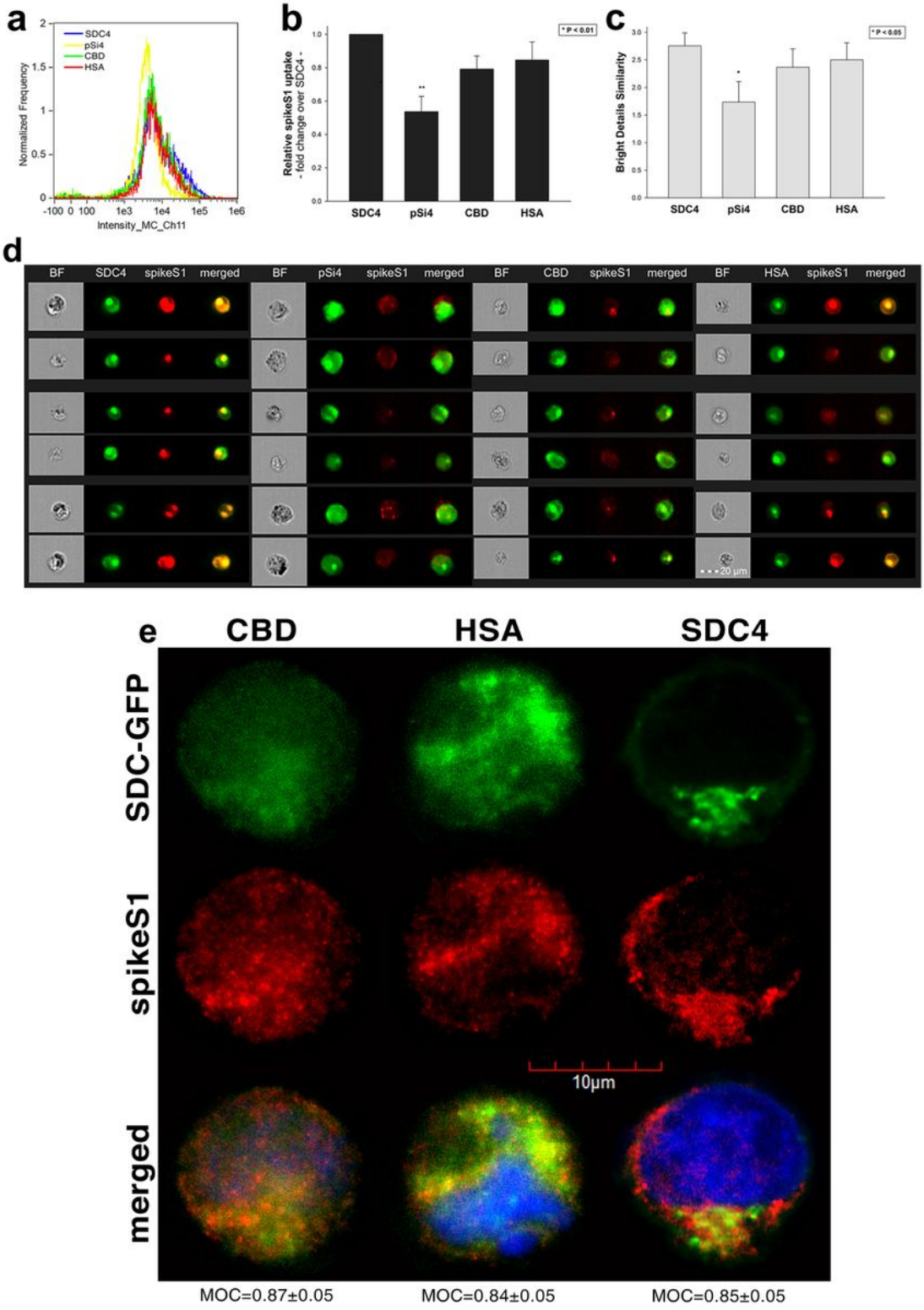

Figure 6

Contribution of the various parts of the SDC4 ectodomain to spikeS1 uptake. (a-d) Results acquired with imaging flow cytometry. (a) Representative flow cytometry histograms showing the intracellular fluorescence of spikeS1-treated SDC4 transfectants and mutants. (b) Detected fluorescence intensities were normalized to spikeS1-treated transfectants expressing WT SDC4 as standards. The bars represent mean ± SEM of four independent experiments. Statistical significance vs spikeS1-treated transfectants

expressing WT SDC4 (standards) was assessed with ANOVA. **p<0.01 vs standards. (c) BDS of spikeS1-treated SDC4 transfectants and mutants. The bars represent mean ± SEM of three independent experiments. Statistical significance vs spikeS1-treated transfectants expressing WT SDC4 as standards was assessed with ANOVA. *p<0.05 vs standards. (d) BF and fluorescent images of spikeS1-treated SDC4 transfectants and mutants. Scale bar = 20 μm. (e) Confocal microscopic visualization of spikeS1-treated CBD, HSA and SDC4 transfectants. Scale bar = 10 μm. MOC ± SEM for the overlap of spikeS1 with CBD, HSA and SDC4 (indicated below the images) was calculated by analysis of 12 images with ~12 cells in each image (from three separate samples).

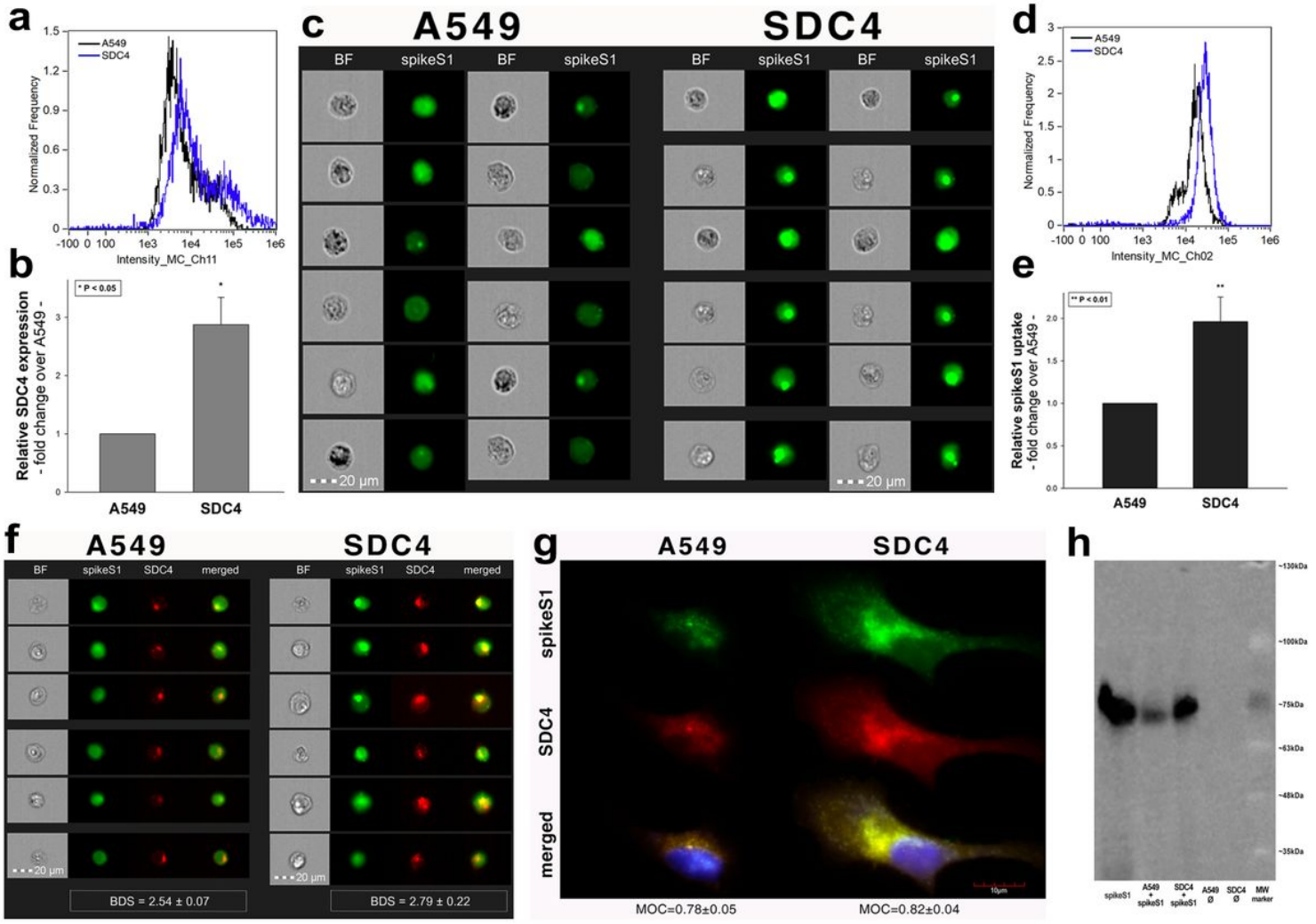

Figure 7

SDC4 overexpression increases spikeS1 uptake A549 cells. WT A549 cells and SDC4 transfectants (created in A549 cells) were incubated with recombinant spikeS1 for 18 h at 37 °C. After incubation, spikeS1-treated cells were trypsinized, fixed, permeabilized and treated with fluorescently labeled anti-His-tag antibodies. After antibody treatment, intracellular fluorescence was analyzed with either imaging flow cytometry or confocal microscopy. (a-b) SDC4 expression measured with flow cytometry by using APC-labeled SDC4 antibodies. (a) Representative flow cytometry histograms showing SDC4 expression levels of WT A549 cells and SDC4 transfectants. (b) Detected SDC4 expression levels were normalized to those

of WT A549 cells as standards. The bars represent mean ± SEM of three independent experiments. Statistical significance vs standards was assessed with ANOVA. *p<0.05 vs standards. (c) Cellular images representing intracellular fluorescence of spikeS1-treated WT A549 cells and SDC4 transfectants (d-e) SDC4 overexpression increases spikeS1 uptake. (d) Representative flow cytometry histograms showing the intracellular fluorescence of spikeS1-treated WT A549 cells and SDC4 transfectants. (e) Fold change in spikeS1 uptake following SDC4 overexpression. The bars represent mean ± SEM of three independent experiments. Statistical significance vs spikeS1-treated WT A549 cells as standards was assessed with ANOVA. **p<0.01 vs spikeS1-treated WT A549 cells as standards. (f) Colocalization of spikeS1 in WT A549 cells and SDC4 transfectants as detected with imaging flow cytometry. The indicated BDS between spikeS1 and SDC4 represents mean ± SEM of three independent experiments. (g) Confocal microscopy visualization of colocalization between spikeS1 and SDC4 in WT A549 cells and SDC4 transfectants. Representative images of three independent experiments are shown. Scale bar = 10 μm. The MOC ± SEM for the overlap of SDC4 with spikeS1 is indicated in the images. The MOC values were calculated by analyzing 12 images with an average of 12 cells in each image (from 3 separate samples). (h) A representative Western blot analysis showing spikeS1 immunoprecipitated with SDC4 in WT A549 cells and SDC4 transfectants. Lane 1: 0.5 ug of spikeS1; Lanes 2-3: immunoprecipitates of spikeS1-treated WT A549 cells and SDC4 transfectants, respectively; Lanes 4-5: immunoprecipitate of WT A549 cells and SDC4 transfectants untreated with spike S1 (controls). Standard protein size markers are indicated on the right.

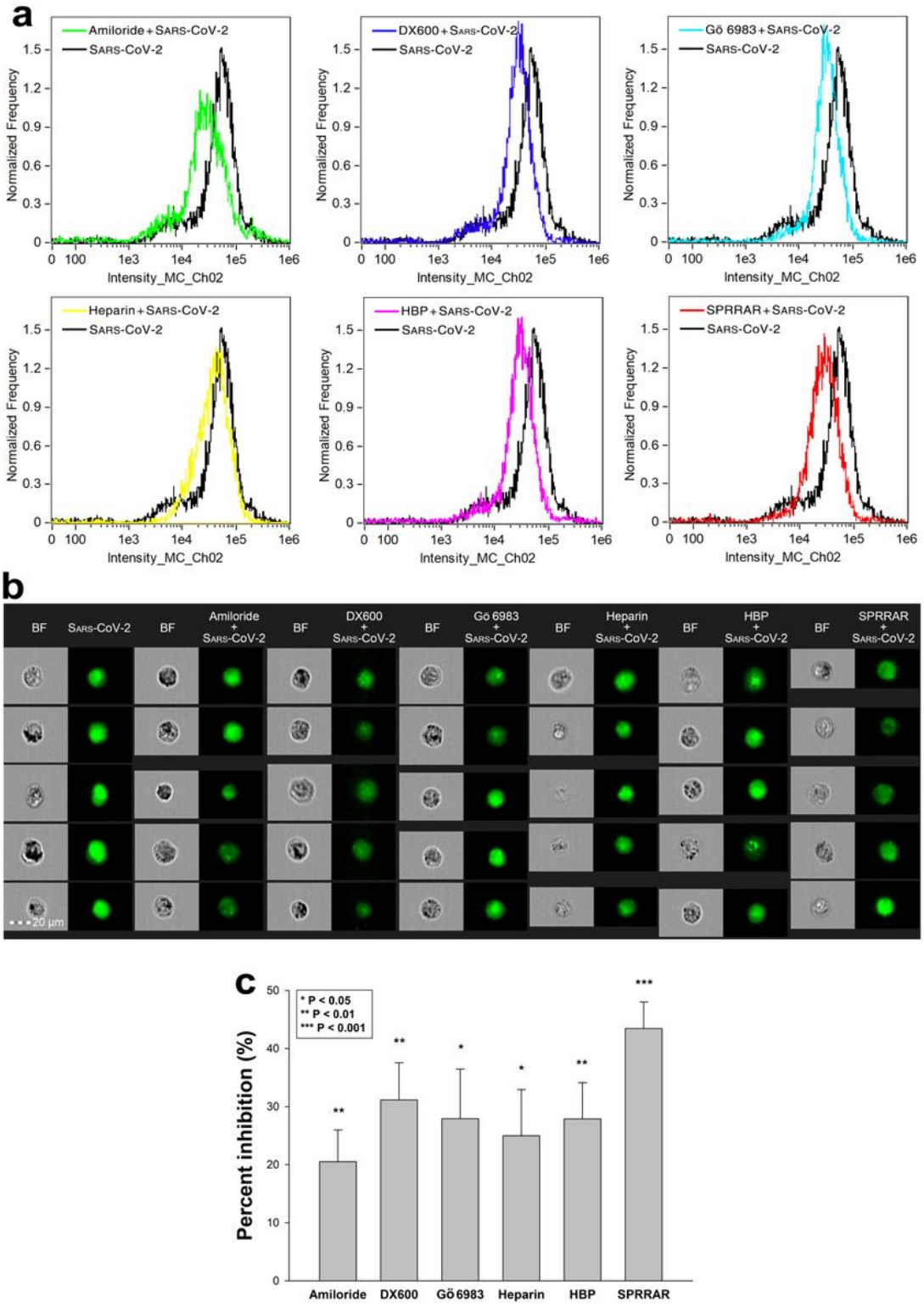

Figure 8

Effects of endocytosis inhibitors on SARS-CoV-2 uptake in A549 cells. (a) Flow cytometry histograms representing intracellular fluorescence of SARS-CoV-2-treated WT A549 cells preincubated with or without either of the following inhibitors: amiloride (100 μM), DX600 (10 μM), Gö 6983 (10 μM), heparin (200 μg/ml), HBP (100 μM) and SPRRAR (100 μM). (b) Cellular images of SARS-CoV-2-treated WT A549 cells preincubated with or without any of the inhibitors. (c) The effect of an inhibitor was expressed as percent

inhibition, calculated with the following formula: [(X − Y)/X] × 100, where X is the fluorescence intensity obtained on cells treated with SARS-CoV-2 in the absence of the inhibitor and Y is the fluorescence intensity obtained on cells treated with SARS-CoV-2 in the presence of inhibitor. The bars represent mean ± SEM of four independent experiments. Statistical significance vs controls treated with SARS-CoV-2 in the absence of the inhibitor was assessed with ANOVA. *p<0.05 vs standards; **p<0.01 vs standards; ***p<0.001 vs standards.

Supplementary Files

This is a list of supplementary files associated with this preprint. Click to download.

- SupplementaryInformationSARSCoV2.pdf